

FREE AND FORCED ION CYCLOTRON WAVES IN A  
CYLINDRICAL CAVITY PARTIALLY FILLED WITH A TWO ION SPECIES PLASMA

M.L. Sawley and M.Q. Tran  
Centre de Recherches en Physique des Plasmas  
Association Euratom - Confédération Suisse  
Ecole Polytechnique Fédérale de Lausanne  
CH-1007 Lausanne / Switzerland

ABSTRACT

Bounded ion cyclotron waves in a cylindrical partially plasma-filled cavity are investigated theoretically using an MHD approach. Both free and forced oscillations are considered. Specific calculations are made for a plasma containing two ion species, with the oscillation frequency in the range between the two ion cyclotron frequencies. The power coupled into the various axial and radial modes from an external antenna is calculated.

## 1. INTRODUCTION

Ion cyclotron waves have been extensively studied in the past due to their application to plasma heating. Experiments conducted at the Princeton laboratory have investigated the absorption of ion cyclotron waves when propagated into a magnetic beach region (see, for example, References 1-7). The waves were launched using a Stix coil<sup>8</sup> whose length, for optimum coupling at the plasma densities examined, was relatively short. Early results<sup>3,4</sup> indicated that a Faraday shield was necessary to eliminate undesired coupling between the coil and the plasma. It was also shown theoretically and experimentally<sup>5,7</sup> that electron inertia may have a dominant influence on ion cyclotron wave propagation, especially for a plasma of low density and a wave frequency close to the ion cyclotron frequency.

The present study was motivated by a proposed experimental investigation<sup>9</sup> of the ponderomotive force exerted by a large amplitude ion cyclotron wave on a plasma containing two ion species.<sup>10-12</sup> This experiment will utilize a plasma having a density much lower than those examined in previous wave heating studies. The parallel wavelength, and hence excitation coil length, is correspondingly much longer and the coupling between coil and plasma significantly different. Wave modes that are bounded in both the axial and the radial direction are to be investigated in the experiment.

In Section 2 the theory for ion cyclotron waves in a cylindrical cavity partially filled with a uniform plasma is outlined. Included in the theory, in particular, are the effects of finite electron mass and the presence of a Faraday shield. Both the free and the forced oscillation problems are treated. With the proposed experiment in mind, in Section 3 the results of specific numerical calculations are presented. For the free oscillation problem, the dependence of the parallel wavenumber on the plasma parameters is examined. In considering forced oscillations, the power deposited into the various radial and axial modes is analyzed, and optimization of power input into a desired mode studied. The radial and axial structures of the wavefields, for both free and forced modes, are calculated.

## 2. THEORY

We shall consider ion cyclotron waves in a uniform cylindrical plasma column of length  $L$  and radius  $p$  imbedded in a uniform axial magnetic field  $B_0$ . The plasma is surrounded by a vacuum region and by a perfectly conducting cylindrical shell of radius  $q$ . The system is bounded in the axial direction by conducting end walls. For the case of forced ion cyclotron waves, we consider excitation by an azimuthal current sheet of radius  $s$  located in the vacuum region. The inclusion of a cylindrical, axially-conducting Faraday shield of radius  $u$  is also considered. A schematic diagram of the resulting partially plasma-filled cavity is shown in Fig. 1.

Small amplitude waves in the partially ionized plasma column may be described by the linearized MHD equations, in which we include the effect due to collisions between the different constituent species, but neglect pressure and viscous terms. A plasma comprised of more than one ion species is treated. We shall consider axisymmetric ( $m = 0$ ) oscillations having a temporal dependence  $\sim \exp(i\omega t)$ . After Fourier analysis in time, Maxwell's equations combine to give for the perturbation electric field

$$\nabla \times (\nabla \times \underline{E}) = \frac{\epsilon^2}{c^2} \underline{K} \cdot \underline{E} \quad (1)$$

where  $\underline{K}$  is the dielectric tensor.

Since the plasma is confined to the region  $-L/2 < z < L/2$ , solutions of eq. (1) for the electric field components may be expressed in terms of finite Fourier series.<sup>13</sup> We write

$$\left. \begin{aligned} E_{r,\theta} &= \sum_{n=1}^{\infty} e_{r,\theta}^n \sin \frac{n\pi}{L} z, \\ E_z &= \frac{1}{2} e_z^0 + \sum_{n=1}^{\infty} e_z^n \cos \frac{n\pi}{L} z. \end{aligned} \right\} \quad (2)$$

These forms have been chosen to satisfy the boundary conditions at the end conducting walls, namely,

$$E_r (z = \pm L/2) = E_\theta (z = \pm L/2) = 0 . \quad (3)$$

Similarly, we write for the magnetic field components

$$\left. \begin{aligned} B_{r,\theta} &= \frac{1}{2} b_{r,\theta}^0 + \sum_{n=1}^{\infty} b_{r,\theta}^n \cos \frac{n\pi}{L} z , \\ B_z &= \sum_{n=1}^{\infty} b_z^n \sin \frac{n\pi}{L} z . \end{aligned} \right\} \quad (4)$$

We proceed by solving eq. (1) in each of the regions shown in Fig. 1.

i) In the plasma : region I

Using the notation of Stix,<sup>8</sup> the dielectric tensor for the plasma may be written as

$$K = \begin{pmatrix} S & -iD & 0 \\ iD & S & 0 \\ 0 & 0 & P \end{pmatrix} . \quad (5)$$

For a fully ionized, collisionless plasma the matrix elements are given by

$$\left. \begin{aligned} S &= 1 - \sum_s \frac{\omega_{ps}^2}{\omega^2 - \omega_{cs}^2} , \\ D &= \sum_s \frac{\omega_{ps}^2 \omega_{cs}}{\omega(\omega^2 - \omega_{cs}^2)} , \\ P &= 1 - \sum_s \frac{\omega_{ps}^2}{\omega^2} , \end{aligned} \right\} \quad (6)$$

where  $\omega_{ps}$  and  $\omega_{cs}$  are, respectively, the plasma frequency and cyclotron frequency for species  $s$ . The elements of the dielectric tensor for a collisional plasma containing three species (electrons, ions and neutrals) have been given by Skipping et al.<sup>13</sup> and for a five species plasma (electrons and two ion and neutral species) by Schlüter and Schürger.<sup>14</sup>

Substituting eq. (5) into (1) using (2) then gives

$$k_{\parallel} \frac{de_z^n}{dr} + (\mathcal{D} - k_{\parallel}^2) e_r^n - i\mathcal{D} e_{\theta}^n = 0, \quad (7)$$

$$\frac{d}{dr} \left( \frac{1}{r} \frac{d}{dr} (r e_{\theta}^n) \right) + (\mathcal{D} - k_{\parallel}^2) e_{\theta}^n + i\mathcal{D} e_r^n = 0, \quad (8)$$

$$k_{\parallel} \frac{1}{r} \frac{d}{dr} (r e_r^n) - \frac{1}{r} \frac{d}{dr} \left( r \frac{de_z^n}{dr} \right) - \mathcal{P} e_z^n = 0, \quad (9)$$

where  $\mathcal{D} = \frac{\omega^2}{c^2} S$ ,  $\mathcal{D} = \frac{\omega^2}{c^2} D$ ,  $\mathcal{P} = \frac{\omega^2}{c^2} P$  (10)

and  $k_{\parallel} = \frac{n\pi}{L}$ . (11)

Considering solutions of eq. (7) - (9) of the form

$$\left. \begin{aligned} e_r^n &= \sum_j A_j^n J_1(k_{\perp j} r), \\ e_{\theta}^n &= \sum_j \epsilon_{2j} A_j^n J_1(k_{\perp j} r), \\ e_z^n &= \sum_j \epsilon_{3j} A_j^n J_0(k_{\perp j} r), \end{aligned} \right\} \quad (12)$$

yields the following dispersion relation

$$\begin{aligned}
 & (\mathcal{D} - k_{\parallel}^2)(\mathcal{D} - k_{\parallel}^2 - k_{\perp j}^2)(k_{\perp j}^2 - \mathcal{P}) \\
 & + k_{\parallel}^2 k_{\perp j}^2 (\mathcal{D} - k_{\parallel}^2 - k_{\perp j}^2) - \mathcal{D}^2 (k_{\perp j}^2 - \mathcal{P}) = 0 . \quad (13)
 \end{aligned}$$

This quadratic equation in  $k_{\perp j}^2$  therefore yields, for each value of  $k_{\parallel}$ , two perpendicular wavenumbers given by

$$k_{\perp j}^2 = \frac{-b \pm (b^2 - 4ac)^{1/2}}{2a} , \quad (14)$$

where

$$\begin{aligned}
 a &= \mathcal{D} \\
 b &= (k_{\parallel}^2 - \mathcal{D})(\mathcal{P} + \mathcal{D}) + \mathcal{D}^2 \\
 c &= \mathcal{P} [(k_{\parallel}^2 - \mathcal{D})^2 - \mathcal{D}^2] .
 \end{aligned}$$

Substituting eq. (2) into (8) and (9) also gives

$$\left. \begin{aligned}
 \epsilon_{2j} &= \frac{i\mathcal{D}}{k_{\parallel}^2 + k_{\perp j}^2 - \mathcal{D}} , \\
 \epsilon_{3j} &= \frac{-k_{\parallel} k_{\perp j}}{k_{\perp j}^2 - \mathcal{P}} .
 \end{aligned} \right\} \quad (15)$$

Using Maxwell's equation  $\nabla \times \underline{E} = i\omega \underline{B}$  and eq. (4), we obtain for the Fourier amplitudes of the perturbation magnetic field components

$$\left. \begin{aligned}
 b_r^n &= \sum_{j=1}^2 \frac{i k_{||}}{\epsilon} \epsilon_{2j} A_j^n J_1(k_{\perp j} r) , \\
 b_\theta^n &= \sum_{j=1}^2 \frac{-i}{\epsilon} (k_{||} + k_{\perp j} \epsilon_{3j}) A_j^n J_1(k_{\perp j} r) , \\
 b_z^n &= \sum_{j=1}^2 \frac{-i}{\epsilon} k_{\perp j} \epsilon_{2j} A_j^n J_0(k_{\perp j} r) ,
 \end{aligned} \right\} \quad (16)$$

for  $n > 1$

and

$$b_r^0 = 0 \quad , \quad b_\theta^0 = \frac{i}{\omega} e_z^0 .$$

ii) In the vacuum region  $k$  ( $k = \text{II} - \text{IV}$ ) :

The fields in each of the vacuum regions may be obtained by setting  $\underline{K} = \underline{I}$  in eq. (1), i.e.,

$$\mathcal{D} = \mathcal{P} = \frac{\epsilon^2}{c^2} \quad , \quad \mathcal{Q} = 0 . \quad (17)$$

We consider solutions for the electric field Fourier amplitudes of the form

$$\left. \begin{aligned}
 e_r^n &= C_k^n I_1(k_0 r) + D_k^n K_1(k_0 r) , \\
 e_\theta^n &= F_k^n I_1(k_0 r) + G_k^n K_1(k_0 r) , \\
 e_z^n &= \frac{k_0}{k_{||}} \left\{ C_k^n I_0(k_0 r) - D_k^n K_0(k_0 r) \right\} ,
 \end{aligned} \right\} \quad (18)$$

which satisfy the vacuum condition,  $\nabla \cdot \underline{E} = 0$ . Substituting eq. (17) and (18) into eq. (7)-(9) yields the following relationship for the vacuum wavenumber,

$$k_o^2 = k_{||}^2 - \frac{\omega^2}{c^2} \quad (19)$$

The magnetic field Fourier amplitudes are then

$$\left. \begin{aligned} b_r^n &= \frac{i}{\omega} k_{||} \left\{ F_k^n I_1(k_o r) + G_k^n K_1(k_o r) \right\}, \\ b_\theta^n &= \frac{-i}{\omega} k_{||} \left( 1 - \frac{k_o^2}{k_{||}^2} \right) \left\{ C_k^n I_1(k_o r) + D_k^n K_1(k_o r) \right\}, \\ b_z^n &= \frac{-i}{\omega} k_o \left\{ F_k^n I_o(k_o r) - G_k^n K_o(k_o r) \right\}. \end{aligned} \right\} \quad (20)$$

The 14 coefficients of the wave amplitudes,

$$A_1^n, A_2^n, C_k^n, D_k^n, F_k^n, G_k^n, \quad k = \text{II, III, IV}$$

are determined by the boundary conditions at the four surfaces,  $r = p, u, s, q$ . At the plasma-vacuum interface, we assume that there are no surface currents or charges (consistent with the inclusion of finite electron mass effects in the description of the plasma). The Faraday shield is assumed to completely eliminate any axial electric field which may be coupled to the plasma from the antenna, while not affecting the azimuthal electric field. The antenna is treated as a current sheet flowing in the azimuthal direction only and having no azimuthal dependence. The imposed current per unit length,  $J^\dagger$ , can be expressed in terms of the following Fourier sine series.



$$J^{\dagger}(z) = \sum_{n=1}^{\infty} j_n^{\dagger} \sin \frac{n\pi}{L} z \quad (21)$$

The cylindrical shell at  $r = q$  is assumed to be perfectly conducting in both the azimuthal and axial directions.

With the above considerations, the appropriate boundary conditions can then be written as follows.

At  $r = p$  :  $E_{\theta}$ ,  $E_z$ ,  $B_{\theta}$  and  $B_z$  are continuous,

$r = u$  :  $E_{\theta}$ ,  $E_z$  and  $B_z$  are continuous

and  $E_z = 0$ ,

$r = s$  :  $E_{\theta}$ ,  $E_z$  and  $B_{\theta}$  are continuous

and  $[B_z]_{r=s} = \mu_0 J^{\dagger}$ ,

$r = q$  :  $E_{\theta} = E_z = 0$ . (22)

Substituting the wavefields expressed in eq. (12), (16), (18) and (20) into the boundary conditions (22) yields the following fourteen equations for the required coefficients of the wave amplitudes.

$$\epsilon_{31} A_1^n J_0(k_{11}p) + \epsilon_{32} A_2^n J_0(k_{12}p) = \frac{k_0}{k_{11}} \left\{ C_{II}^n I_0(k_0p) - D_{II}^n K_0(k_0p) \right\},$$

$$(k_{11} + k_{11}\epsilon_{31}) A_1^n J_1(k_{11}p) + (k_{11} + k_{12}\epsilon_{32}) A_2^n J_1(k_{12}p)$$

$$= k_{11} \left( 1 - \frac{k_0^2}{k_{11}^2} \right) \left\{ C_{II}^n I_0(k_0p) + D_{II}^n K_0(k_0p) \right\},$$

$$\epsilon_{21} A_1^n J_1(k_{11} \rho) + \epsilon_{22} A_2^n J_1(k_{12} \rho) = F_{\text{II}}^n I_1(k_0 \rho) + G_{\text{II}}^n K_1(k_0 \rho),$$

$$\epsilon_{21} k_{11} A_1^n J_0(k_{11} \rho) + \epsilon_{22} k_{12} A_2^n J_0(k_{12} \rho) = k_0 \left\{ F_{\text{II}}^n I_0(k_0 \rho) - G_{\text{II}}^n K_0(k_0 \rho) \right\},$$

$$C_{\text{II}}^n I_0(k_0 u) - D_{\text{II}}^n K_0(k_0 u) = 0,$$

$$C_{\text{III}}^n I_0(k_0 u) - D_{\text{III}}^n K_0(k_0 u) = 0,$$

$$F_{\text{I}}^n I_1(k_0 u) + G_{\text{I}}^n K_1(k_0 u) = F_{\text{III}}^n I_1(k_0 u) + G_{\text{III}}^n K_1(k_0 u),$$

$$F_{\text{II}}^n I_0(k_0 u) - G_{\text{II}}^n K_0(k_0 u) = F_{\text{III}}^n I_0(k_0 u) - G_{\text{III}}^n K_0(k_0 u),$$

$$C_{\text{II}}^n I_0(k_0 s) - D_{\text{II}}^n K_0(k_0 s) = C_{\text{IV}}^n I_0(k_0 s) - D_{\text{IV}}^n K_0(k_0 s),$$

$$C_{\text{III}}^n I_1(k_0 s) + D_{\text{III}}^n K_1(k_0 s) = C_{\text{IV}}^n I_1(k_0 s) + D_{\text{IV}}^n K_1(k_0 s),$$

$$F_{\text{III}}^n I_1(k_0 s) + G_{\text{III}}^n K_1(k_0 s) = F_{\text{IV}}^n I_1(k_0 s) + G_{\text{IV}}^n K_1(k_0 s),$$

$$\left\{ F_{\text{II}}^n - F_{\text{IV}}^n \right\} I_0(k_0 s) - \left\{ G_{\text{II}}^n - G_{\text{IV}}^n \right\} K_0(k_0 s) = \frac{i \omega \mu_0}{k_0} j_n^{\dagger},$$

$$C_{\text{IV}}^n I_0(k_0 q) - D_{\text{IV}}^n K_0(k_0 q) = 0,$$

$$F_{\text{IV}}^n I_1(k_0 q) + G_{\text{IV}}^n K_1(k_0 q) = 0. \quad (23)$$

It should be noted that the removal of the Faraday shield may be easily achieved by setting  $E_{\theta}$ ,  $E_z$ ,  $B_{\theta}$  and  $B_z$  to be continuous at  $r = u$ .

The fifth and sixth equations of the set (23) are then replaced by

$$C_{\text{II}}^{\text{n}} I_0(k_0 u) - D_{\text{II}}^{\text{n}} K_0(k_0 u) = C_{\text{III}}^{\text{n}} I_0(k_0 u) - D_{\text{III}}^{\text{n}} K_0(k_0 u) ,$$

$$C_{\text{II}}^{\text{n}} I_1(k_0 u) + D_{\text{II}}^{\text{n}} K_1(k_0 u) = C_{\text{III}}^{\text{n}} I_1(k_0 u) + D_{\text{III}}^{\text{n}} K_1(k_0 u) .$$

The set of equations (23) may be written more compactly in matrix form:

$$[ M ] [ X ] = [ B ] , \quad (24)$$

where

[ M ] is a 14 x 14 complex banded matrix with seven nonzero diagonals,

[ X ] is a 14 x 1 complex column matrix containing the unknown coefficients of the wave amplitudes,

[ B ] is a 14 x 1 complex column matrix containing the right-hand side forcing term.

For the free oscillation problem, [ B ] is zero and eq. (24) has a nontrivial solution if and only if

$$\det [ M ] = 0. \quad (25)$$

Solving the free oscillation problem is therefore an eigenvalue problem for which one searches for eigenvalues satisfying eq. (25). There is, in general, for each value of n (and therefore,  $k_{\parallel}$ ), an infinite set of eigenvalues corresponding to the different radial modes of oscillation of the plasma column. For the special case of a collisionless plasma, the eigenvalues are all real. One may therefore treat,

for example, the oscillation frequency  $\omega$ , the plasma density  $n_e$ , or the plasma radius  $p$ , as the eigenvalue characterizing the oscillation and hold all other parameters fixed. However, for a collisional plasma, the eigenvalues are all complex, reflecting the damped behaviour of the eigenmodes. For this case, it is convenient to treat  $\omega$  as the complex eigenvalue, its imaginary part characterizing the damping rate of the oscillation.

For the forced oscillation problem, eq. (24) can be solved to give the coefficients of the wave amplitudes, and therefore the oscillation field structure. Of particular importance for this case is the power coupled from the antenna to the plasma. Collisions in the plasma will result in a net flow of energy into the plasma. The complex power input to the plasma-antenna system, averaged over one period of oscillation, is given by<sup>15</sup>

$$\langle P \rangle = \frac{1}{2} \int_V \underline{J}^\dagger \cdot \underline{E} \, dV, \quad (26)$$

where the integral is calculated over the volume of the antenna. If the plasma loading of the antenna is modelled by a complex impedance in series with the impedance of the antenna, then we may also write the power input as

$$\langle P \rangle = \frac{1}{2} I_0^2 \left\{ R_c + R_p - i\omega(L_c + L_p) \right\}, \quad (27)$$

where  $R_c, L_c$  are the antenna resistance and inductance,  
 $R_p, L_p$  are the resistive and reactive components of  
the plasma loading,  
and  $I_0$  is the amplitude of the antenna current.

The resistive and reactive components of the power input to the plasma are, respectively,

$$P_R = \frac{1}{2} I_0^2 R_p \quad ; \quad P_I = \frac{1}{2} I_0^2 \omega L_p. \quad (28)$$

For an antenna consisting of a coil wound with  $v(z)$  turns per unit length, then

$$J^{\dagger}(z) = I_0 v(z) . \quad (29)$$

By substituting the Fourier expansion of the antenna current density, eq. (21), and the electric field at the antenna, eq. (2), into (26), the power input to the  $n^{\text{th}}$  axial mode can be obtained.

$$\begin{aligned} \langle P^n \rangle &= \frac{1}{2} 2\pi s \int_{-L/2}^{L/2} \left\{ \sum_{m=1}^{\infty} j_n^{\dagger} e_{\theta}^m(s) \sin \frac{n\pi z}{L} \sin \frac{m\pi z}{L} \right\} dz \\ &= \frac{\pi s L}{2} j_n^{\dagger} e_{\theta}^n(s) . \end{aligned} \quad (30)$$

### 3. NUMERICAL EXAMPLES

Using the theory outlined in Section 2, we shall examine both free and forced ion cyclotron waves in a partially ionized neon plasma containing two isotopic species,  $\text{Ne}^{20}$  and  $\text{Ne}^{22}$ , in approximately their natural relative abundance ( $n_1 = 90.7\%$  and  $n_2 = 9.3\%$ , respectively). The plasma parameters, unless otherwise specified, are as follows:

electron density,  $n_e = 10^{10} \text{ cm}^{-3}$

axial magnetic field,  $B_0 = 0.3 \text{ T}$

ion cyclotron frequencies,  $\omega_{c1} = 1.447 \times 10^6 \text{ rad s}^{-1}$   
(230.4 kHz)

$\omega_{c2} = 1.316 \times 10^6 \text{ rad s}^{-1}$   
(209.4 kHz)

plasma radius,  $p = 2.5 \text{ cm}$

conducting shell radius,  $q = 20 \text{ cm}$

plasma length,  $L = 5.4 \text{ m}$

and for the case of forced oscillation,

$$\begin{aligned} \text{antenna radius,} & \quad s = 6 \text{ cm} \\ \text{Faraday shield radius,} & \quad u = 5 \text{ cm} \end{aligned} \quad (31)$$

The above set of parameters have been chosen to model those expected in the LMP device<sup>9</sup>, presently under construction at the CRPP, in which the ponderomotive force exerted by a large amplitude ion cyclotron wave on a plasma with two ion species is to be investigated. The plasma formed in this device will be weakly ionized (percentage ionization  $\sim 0.1\%$ ) and cold ( $T_i \sim 0.1 \text{ eV}$ ,  $T_e \sim 2-5 \text{ eV}$ ). Therefore the dominant dissipative mechanism for a wave of frequency sufficiently far from each of the ion cyclotron frequencies (that is,

$$|\omega - \omega_{ci}| \gg k_{\parallel} v_{th}^i, \quad (32)$$

where  $v_{th}^i$  is the ion thermal speed of species  $i$ ) is ion-neutral collisions. The approach adopted to treat the effect of collisions is outlined in Appendix A. Since the main objective of the present study is to investigate forced ion cyclotron waves, for reason of simplicity of the calculations the presence of collisions is neglected for the free oscillation problem ( $\omega$  and  $k_0$  are real). For the calculation of the forced oscillations, ion-neutral collisions are assumed to be the sole dissipative mechanism, with an

effective ion-neutral collision frequency,  $\nu_{in} = 5.8 \text{ kHz}$ .

### 3.1 Free ion cyclotron waves

Before examining specific examples of the bounded free oscillation problem we first consider the relationship between the parallel and perpendicular wavenumbers given by the plasma dispersion relation, eq. (13). (This relationship is independent of the nature of the plasma boundaries, however, the boundary conditions will determine the discrete values of wavenumbers that are allowable.) We consider oscillations having a frequency between the two ion cyclotron frequencies,  $\omega = 1.372 \times 10^6 \text{ rad s}^{-1}$ .

In Fig. 2 is plotted the curve calculated from the dispersion relation. This graph clearly shows the two branches corresponding to the fast (magnetoacoustic) and slow (ion cyclotron) waves. We shall confine the present study to the latter branch, and will be interested in parallel wavenumbers of the order of unity. It can be noted from Fig. 2 that under these conditions one of the perpendicular wavenumbers has a much larger amplitude than the other. The larger perpendicular wavenumber, denoted by  $k_{\perp 1}$ , is always real for the plasma under consideration.

We now consider a plasma column of radius  $p$ , but unbounded in the axial direction. The plasma is separated from a conducting shell of radius  $q$  by a vacuum region. In Fig. 3, 4 and 5 are shown graphs of the parallel wavenumber,  $k_{\parallel}$ , as a function of the wave frequency,  $\omega$ , the electron density,  $n_e$ , and the plasma radius,  $p$ , respectively. Where not specified, the plasma parameters are the same as for Fig. 2. In each of Fig. 3 - 5 are displayed curves for the lowest four radial modes, i.e.,  $\ell = 1, 2, 3, 4$ . The radial mode number is approximately related to the dominant perpendicular wavenumber through the relation (see Appendix B)

$$k_{\perp 1} p = \alpha_{\ell} \quad , \quad (33)$$

where  $\alpha_{\ell}$  is the  $\ell$ th zero of the  $J_{\ell}$  Bessel function.

Figure 3 shows that, for the present parameter values, the wave resonance at the cyclotron frequency of the minority species (i.e.,  $\text{Ne}^{22}$ ) is very sharp, and that for most frequencies in the range between the two cyclotron frequencies the wave is propagating (i.e.,  $k_{\parallel}$  is real). For a given fixed frequency the magnitude of the axial wavenumber increases with increasing radial mode number: waves of higher radial mode number propagate with smaller axial wavelengths.

For a fixed wave frequency, Fig. 4 demonstrates the strong dependence of the parallel wavenumber on the radius of the plasma column. As shown in Appendix B,  $k_{\parallel}$  is approximately inversely proportional to the plasma radius: a plasma column of small radius can support a propagating ion cyclotron wave having a short axial wavelength.

The axial wavelength of an ion cyclotron wave propagating with a given frequency in a plasma column of fixed radius is independent of the density of the plasma over a wide range of density (see Appendix B). For the plasma parameters used in the present study, Fig. 5 shows that the axial wavenumber is constant for  $2 \times 10^7 < n_e < 2 \times 10^{11} \text{ cm}^{-3}$ , i.e. 4 decades in density. For lower density, the wavenumber increases as the density approaches that corresponding to the plasma cutoff  $P = 0$  (i.e.,  $n_e = 6 \times 10^2 \text{ cm}^{-3}$ ). The wavenumber also increases for higher densities, so that the axial wavelength is significantly shorter in the density regime of previous experiments<sup>1-7,16</sup>.

If the axial boundary conditions at  $z = \pm L/2$  are imposed, only discrete values of axial wavenumber are allowable. Each eigenmode of the cavity is then characterized by an axial mode number,  $n$  (related to  $k_{\parallel}$  by eq. (11)), in addition to the radial mode number,  $\ell$ .

For the parameters given in (31), graphical determination of the frequencies of oscillation for the lowest order eigenmodes is shown in Fig. 6. A table of values, obtained numerically, is given in Table 1.

If an eigenfrequency midway between the two ion cyclotron frequencies is desired (to satisfy (32) and therefore minimize ion cyclotron damping of the wave), Fig. 6 shows that a good choice of eigenmode is the  $(n = 4, \ell = 1)$  mode. This mode has an eigenfrequency  $\omega = 1.381 \times 10^6 \text{ rad s}^{-1}$ . (For the experiment to be conducted on the LMP device, this mode also has the advantages of a field structure with a simple radial dependence and an axial dependence that is convenient for diagnostic access.) Radial and axial profiles of the amplitude of the electric and magnetic field components for this eigenmode are shown in Fig. 7. The amplitude of the fields have been normalized to provide an axial electric field of  $10 \text{ Vm}^{-1}$  on the plasma axis at the axial antinodes. It can be seen that this mode is almost purely linearly polarized, with the dominant electric field component being the radial component. The inclusion of the effect of electron inertia in the calculations is seen to produce a non-negligible component of electric field in the axial direction:  $|E_z|_{\text{max}} \sim 0.026 |E_r|_{\text{max}}$ . (The axial electric field is short-circuited by the electrons if they are assumed to have zero mass.)



For a given set of plasma parameters, the eigenfrequency for a selected mode is fixed. If it is required to change this frequency (for example, to study the influence on nonlinear effects of the difference of the frequency and the cyclotron frequency of one of the plasma species<sup>9</sup>) one or more of the plasma parameters must be changed. For the set of parameters given in (31), Fig. 5 shows that a change in the electron density will not produce a significant change in the eigenfrequency. The eigenfrequency may be altered by changing the radius of the plasma, as indicated by Fig. 4, however experimentally, this may not be easy to do. Changing the strength of the axial magnetic field  $B_0$  produces a change in the cyclotron frequencies in addition to a change in the eigenfrequencies in such a manner that the ratio  $(\omega_{ci} - \omega)/\omega_{ci}$  remains approximately constant: it is therefore not possible to set the eigenfrequency arbitrarily close to a cyclotron frequency without drastically affecting the nature of the plasma. An effective change of the eigenfrequency may be achieved, however, by altering the isotopic concentration of the plasma. Figure 8 shows a plot of the eigenfrequency of the  $(n = 4, \ell = 1)$  mode as a function of the percentage concentration of the  $\text{Ne}^{20}$  species. The value calculated for the natural concentration is marked by a dot on the curve. It can be seen that by decreasing the percentage concentration of the  $\text{Ne}^{20}$  species the eigenfrequency can be made to approach the cyclotron frequency for this ion species.

### 3.2 Forced ion cyclotron waves

We now consider forced oscillation of the bounded plasma column by means of an oscillating azimuthal current in the vacuum region, as described in section 2. If plasma dissipative effects are sufficiently small, exciting the column with a frequency close to one of the eigenfrequencies will result in large internal wavefields and substantial resistive power coupling from the antenna to the plasma. In this section, we shall concentrate our attention on the excitation of the  $(n = 4, \ell = 1)$  mode.

An appropriate choice for the antenna is one that closely approximates the axial structure of the desired mode. It should be noted that with an external antenna there is no geometrically determined control of the radial structure of the mode that is preferentially excited: control is obtained by tuning the oscillation frequency to match that of the required mode. We shall consider an antenna which consists of four separate coils and has a current distribution given by

$$J^{\dagger}(z) = \begin{cases} I_0 v_0 & \text{for } -\frac{3b}{2} - \frac{a}{2} \leq z \leq -\frac{3b}{2} + \frac{a}{2} \\ & \frac{b}{2} - \frac{a}{2} \leq z \leq \frac{b}{2} + \frac{a}{2} \\ -I_0 v_0 & \text{for } -\frac{b}{2} - \frac{a}{2} \leq z \leq -\frac{b}{2} + \frac{a}{2} \\ & \frac{3b}{2} - \frac{a}{2} \leq z \leq \frac{3b}{2} + \frac{a}{2} \\ 0 & \text{otherwise,} \end{cases} \quad (34)$$

with a coil width,  $a$ , and separation,  $b$ , given by

$$\begin{aligned} a &= \lambda/4 = 67.5 \text{ cm} \\ b &= \lambda/2 = 135 \text{ cm} \end{aligned}$$

where  $\lambda$  is the periodicity length of the antenna structure ( $2\lambda=L=5.4\text{m}$ ). A schematic diagram of the antenna is given in Fig. 9.

The Fourier spectrum of the antenna current (and therefore also of the vacuum wavefield excited by this antenna), given by eq. (21), is

$$j_n^{\dagger} = \frac{16}{n\pi} I_0 v_0 \sin\left(\frac{n\pi a}{2L}\right) \sin\left(\frac{n\pi}{8}\right) \cos\left(\frac{n\pi}{4}\right) \cos\left(\frac{n\pi}{2}\right) \quad (35)$$

and is shown in Fig. 10(a) for mode numbers up to  $n = 55$ . Due to the symmetry of the antenna, contributions to the antenna current exist from only every eight axial mode. However, it can be seen from Fig. 10(a) that there is a substantial contribution to the current from these higher order components.

Choosing a value for the coil current turns per unit length,  $I_0 v_0$ , and using eq. (30) and (35), the power coupled from the antenna to each of the axial modes may be calculated. We shall consider

$$I_0 v_0 = 2.963 \times 10^3 \text{ Am}^{-1}$$

corresponding for the LMP experiment to a current of 80 A and coils with 25 turns per 67.5 cm.

Figure 11 shows the dependence on frequency of the resistive and reactive components of the power coupled from the antenna to the  $n = 4$  mode. A strong peak is observed at the frequency of oscillation that equals the eigenfrequency for the  $(n = 4, \ell = 1)$  mode. A much weaker peak, corresponding to resonant excitation of the  $(n = 4, \ell = 2)$  mode, is observed at a lower value of frequency. The resonance peaks for the higher order radial modes are not discernible.

It should be noted that the maximum power input to the plasma of  $P_R = 0.74$  watts, which occurs at the resonance frequency of the  $(n = 4, \ell = 1)$  mode, corresponds to a plasma resistance of  $R_p = 0.23 \text{ m}\Omega$ . This is much less than the resistance that is typical for the antenna being considered ( $R_C$  of the order of  $0.1 \Omega$ ). Hence, in an experimental situation, most of the generator power is expected to be dissipated in the antenna resistance. In fact, for an antenna having a resistance of  $R_C = 0.3 \Omega$ , 960 watts is dissipated in the antenna if the assumed current of 80 A is flowing. In addition, the change in reactive power due to the presence of the plasma is much less than the vacuum reactive power. For the antenna being considered, the vacuum inductance is  $L_C = 45.5 \mu\text{H}$  corresponding to a reactive power at a frequency of  $\omega = 1.381 \times 10^6 \text{ rad s}^{-1}$  of  $2.01 \times 10^5$  watts.

Figure 10(b) shows the resistive power input to the different axial modes for a driving frequency fixed at the eigenfrequency for the  $(n = 4, \ell = 1)$  mode,  $\omega = 1.381 \times 10^6 \text{ rad s}^{-1}$ . It can be seen from this plot that nearly all of the power (99.1%) is deposited in the  $n = 4$  mode: there is only a weak coupling at this frequency between the antenna and plasma for the non-zero higher order Fourier components of the antenna current. Thus, Fig. 10(b) and 11 show that by

tuning the driving frequency, very selective excitation of the desired ( $n = 4, \ell = 1$ ) mode may be obtained.

Radial and axial profiles of the electric and magnetic field components for excitation at a frequency  $\omega = 1.381 \times 10^6$  rad s<sup>-1</sup> are plotted in Fig. 12. These fields were obtained by summing the contributions from the first 100 axial modes, i.e.,  $1 \leq n \leq 100$ . The effect of a Faraday shield was not included. For the parameters chosen for the present study, the field components  $E_\theta$ ,  $B_r$  and  $B_z$  are essentially the vacuum field of the antenna: there is negligible modification to these components due to the presence of the plasma. The remaining three field components  $E_r$ ,  $E_z$  and  $B_\theta$ , which are zero in the absence of a plasma, can be seen to exhibit radial and axial structure very similar to the ( $n = 4, \ell = 1$ ) eigenmode (c.f. Fig. 7). This shows that this mode is selectively excited. In the plasma region ( $0 < r < \rho$ ), the major component of the electric field is the radial component, which reaches a maximum value of  $|E_r| = 344$  Vm<sup>-1</sup> near the mid-radius position.

Figure 13 shows the effect on the wavefields of the presence of a Faraday shield. In this figure is plotted the radial profiles of the electric and magnetic field components. It can be seen that the shield has a negligible effect on the wavefields in the plasma region, but eliminates the radial and axial components of the electric field in the vacuum region between the shield and the conducting wall. The shield can therefore act to decouple the axial electric field of a non-ideal antenna from the plasma. It should be noted that the presence of a Faraday shield does not affect the power coupled to the plasma from the idealized antenna considered in this paper.

The power coupled to the plasma will depend on the distance of the antenna from the plasma surface. To obtain the maximum power coupling the antenna is required to be placed as near as possible to the plasma. Experimentally, there is a lower limitation on the plasma-antenna spacing due to the possibility of undesired effects (e.g., breakdown, corona) and perhaps the necessity of a Faraday shield. To evaluate a compromise between these competing considerations, in Fig. 14 is plotted the resistive power coupled to the plasma at the

( $n = 4$ ,  $\ell = 1$ ) resonance frequency as a function of the position of the antenna. There is a smooth, monotonic decrease in power as the antenna is moved away from the plasma due to the influence of the conducting wall on the wavefields in the cavity. For an antenna radius of  $s = 6$  cm chosen for the calculations shown in the previous figures, the power coupled to the plasma is 85% of the value obtained if the antenna were situated at the plasma boundary,  $p = 2.5$  cm.

We have considered so far a cavity which has a length equal to an integer times the periodicity length of the antenna, namely,  $L = 2\lambda$ . To determine the effect of some mismatch between the antenna periodicity and the cavity length, calculations have been made for a cavity of reduced length,  $L = 4.75$  m, while maintaining the same antenna dimensions: that is,  $L = 1.76\lambda$ . (These calculations have been motivated by the fact that the length of the region of homogeneous magnetic field in the LMP device is less than twice the desired periodicity length of the antenna set by radial access between the magnetic field coils.) Altering the length of the cavity changes the Fourier spectrum of  $k_{\parallel}$ , given by eq. (11). From Fig. 6 it can be seen that if we still consider the ( $n = 4$ ,  $\ell = 1$ ) mode, decreasing the value of  $L$  will result in an increase in the eigenfrequency for this mode. For  $L = 4.75$  m, we obtain  $\omega = 1.393 \times 10^6$  rad s<sup>-1</sup> (c.f.  $\omega = 1.381 \times 10^6$  rad s<sup>-1</sup> for  $L = 5.4$  m). Retaining the same antenna dimensions as was used for the previous calculations means that the Fourier spectrum of the antenna current will now contain more non-zero components. The spectrum is graphically displayed in Fig. 15(a). Due to the mismatch between the antenna periodicity and the cavity length, all even values of axial mode number are now non-zero. The resistive power input to the different axial modes at the resonance frequency for the ( $n = 4$ ,  $\ell = 1$ ) mode is plotted in Fig. 15(b). It can be observed that decreasing the cavity length does not significantly reduce the selectivity of the antenna: almost all of the power (97.1%) is deposited in the  $n = 4$  mode. Comparing Fig. 15(b) with Fig. 10(b) also shows that decreasing the cavity length does not result in a significant reduction in the total power input to the plasma. In Fig. 16 is plotted the radial and axial profiles of the amplitude of the electric field for this forced mode. Comparing these curves with those of Fig. 12(a) shows that the general characteristics of the wavefields are preserved if the cavity

length is decreased. Only a small decrease in the magnitude of the radial and axial components of the electric field in the plasma region is observed.

#### 4. CONCLUSIONS

Calculations made for ion cyclotron waves in a plasma containing two ion species show that for low density and a frequency approximately midway between the two ion cyclotron frequencies, the axial wavelength is much longer than has been examined in experiments to date. For the low density regime considered in this paper, the power input to the plasma, assuming a reasonable value for the collisional damping rate, is small: the power dissipated in the antenna resistance would, in an experimental situation, be much larger. However, the wavefields associated with the ion cyclotron mode excited by the antenna are of the same order of magnitude as the vacuum wavefields. The present calculations have shown that with a judicious choice of antenna design and excitation frequency a very pure bounded mode may be excited. This preferential excitation does not appear to be very sensitive on the length of the plasma cavity.

APPENDIX A

Inclusion of collisions in the theory for ion cyclotron waves in a plasma containing two ion species.

In general, the linearized equation of motion for each plasma species may be written as

$$-i\omega m_s n_s \underline{v}_s = \epsilon_s e n_s [\underline{E} + \underline{v}_s \times \underline{B}_0] - \nabla \cdot \underline{\Pi}_s - \sum_{t \neq s} \underline{P}_{st} \quad , \quad (\text{A.1})$$

where

$$\epsilon_s = \begin{cases} -1 & \text{for electrons} \\ 0 & \text{neutrals} \\ 1 & \text{single ionized ions.} \end{cases}$$

The viscous stress term  $\nabla \cdot \underline{\Pi}_s$  relates the momentum transfer due to the self-collision of particles of species  $s$ , while the rate of momentum transfer from species  $s$  to species  $t$  is given by

$$\underline{P}_{st} = m_s n_s \underline{v}_{st} (\underline{v}_s - \underline{v}_t) \quad .$$

To evaluate the relative importance of the various types of collisions, we first note that for an ion cyclotron wave the dominant fluid velocity is in the perpendicular direction, with

$$|\underline{v}_{s\perp}| \sim \frac{|E_{\perp}|}{B_0} \frac{\omega_{cs}}{(\omega_{cs} - \omega)} \quad . \quad (\text{A.2})$$

The dominant component of the viscous stress term is then due to perpendicular momentum transfer across the equilibrium magnetic field lines. Therefore we have<sup>17</sup>

$$\nabla \cdot \underline{\Pi}_s \sim \frac{\partial}{\partial r} \eta_{\perp}^s \frac{\partial V_{s\perp}}{\partial r}, \quad (\text{A.3})$$

where  $\eta_{\perp}^s$  is the perpendicular viscosity coefficient given by (for  $\omega_s \tau_s \gg 1$ ):

for ions

$$\begin{aligned} \eta_{\perp}^i &= \frac{0.31 \eta_0^i}{(\omega_{ci} \tau_i)^2} \\ \eta_0^i &= 1.94 \times 10^{-23} n_i T_i \tau_i \\ \tau_i &= \frac{1.14 \times 10^7 A^{1/2} T_i^{3/2}}{n_i \ln \Lambda}, \end{aligned}$$

for electrons

$$\begin{aligned} \eta_{\perp}^e &= \frac{0.70 \eta_0^e}{(\omega_{ce} \tau_e)^2} \\ \eta_0^e &= 1.85 \times 10^{-23} n_e T_e \tau_e \\ \tau_e &= \frac{2.66 \times 10^5 T_e^{3/2}}{n_e \ln \Lambda}. \end{aligned}$$

(A.4)

The collision frequencies for momentum transfer between ions and electrons<sup>18</sup>, ions and neutrals<sup>19</sup>, and electrons and neutrals<sup>20</sup> are given by

$$\begin{aligned} \nu_{ie} &= 1.99 \times 10^{-9} n_i T_e^{-3/2} A^{-1} \ln \Lambda \\ \nu_{in} &= 96.9 n_n Q_D \left( \frac{T_i}{A} \right)^{1/2} \\ \nu_{en} &= 1.48 \times 10^3 n_n Q_D T_e^{1/2}, \end{aligned} \quad (\text{A.5})$$





It should be noted that since  $n_n \gg n_i$  and  $v_{in} \ll \omega$ , the neutrals do not effectively couple into the wave motion.

The ratio of the corresponding momentum transfer rates is therefore

$$\frac{\nabla \cdot \Pi_i}{P_{in}} \sim \frac{\eta_i}{p^2} \frac{1}{m_i n_i v_{in}} = 1.6 \times 10^{-3}$$

$$\frac{\nabla \cdot \Pi_e}{P_{in}} \sim 1.6 \times 10^{-10}$$

$$\frac{P_{ie}}{P_{in}} \sim 1.6 \times 10^{-3}$$

$$\frac{P_{en}}{P_{in}} \sim 2.6 \times 10^{-5}$$

(A.7)

The dominant collisional mechanism for this plasma, which has parameters characteristic of those of interest in the present study, is therefore ion-neutral collisions.

Under these conditions, the equation of motion for the ions in a plasma containing two ion species may be written as

$$-i\omega m_i \underline{v}_i = e \left[ \underline{E} + \underline{v}_i \times \underline{B}_0 \right] - m_i v_{in} \underline{v}_i, \quad (A.8)$$

$i = 1, 2$

where  $v_{in}$  is the total ion-neutral collision frequency for collisions between ion species  $i$  and both of the neutral fluids, that is,

$$v_{in} = v_{in1} + v_{in2}.$$

For ion species with approximately the same mass and temperature, the total ion-neutral collision frequency has the same value. Equation (A.8) can then be rewritten as

$$-i\omega m_i^* \underline{v}_i = e \left[ \underline{E} + \underline{v}_i \times \underline{B}_0 \right], \quad (\text{A.9})$$

where the effective complex ion mass  $m_i^*$  is given by

$$m_i^* = m_i \left( 1 + i \frac{\nu_{in}}{\omega} \right). \quad (\text{A.10})$$

The effect of ion-neutral collisions can therefore be taken into account by replacing the ion mass for each ion species by the above complex ion mass in the elements of the dielectric tensor listed in eq. (6).

APPENDIX B

Approximate ion cyclotron wave relationships

The dispersion relation for a hydromagnetic wave in a uniform, magnetized plasma can be written, by re-arranging eq. (13), in the form

$$k_{\parallel}^2 - \mathcal{D} = -\frac{(\mathcal{D} + \rho)}{2\rho} k_{\perp j}^2 \left\{ 1 \mp \left[ 1 - \frac{4\rho\mathcal{D}k_{\perp j}^4 + 4\rho\mathcal{D}^2(k_{\perp j}^2 - \rho)}{(\mathcal{D} + \rho)^2 k_{\perp j}^4} \right]^{1/2} \right\} . \quad (\text{B.1})$$

$j = 1, 2$

If  $k_{\perp j}^2 \gg \frac{\mathcal{D}^2}{\rho}$  ;  $\mathcal{D} \left| \frac{\rho}{\mathcal{D}} \right|^{1/2}$  , (B.2)

the two perpendicular wavenumbers are then related to the parallel wavenumber through the relations

$$k_{\perp a}^2 = \frac{\rho}{\mathcal{D}} (\mathcal{D} - k_{\parallel}^2) \quad (\text{B.3a})$$

$$k_{\perp b}^2 = \mathcal{D} - k_{\parallel}^2 . \quad (\text{B.3b})$$

Since  $|\rho| \gg \mathcal{D}$  for the cases of interest in the present study, we have that  $|k_{\perp a}| \gg |k_{\perp b}|$ . According to the nomenclature adopted in eq. (14) (see Fig. 2),  $k_{\perp a} \approx k_{\perp 1}$  for the slow wave, while  $k_{\perp a} \approx k_{\perp 2}$  for the fast wave. We shall confine our attention to the slow wave (ion cyclotron) branch.

The inequalities (B.2) are satisfied over a wide range of parameters. From eq. (B.3a) we therefore have, to a good approximation,

$$k_{\parallel}^2 = \mathcal{D} \left( 1 - \frac{k_{\perp}^2}{\rho} \right) . \quad (\text{B.4})$$

It should be noted, however, that the inequalities (B.2) are clearly not satisfied if  $\mathcal{D} = 0$ . This occurs for a plasma containing two ion species when the wave frequency equals the ion-ion hybrid frequency,  $\omega_{\text{IIH}}$ , which is given by<sup>22</sup>

$$\omega_{\text{IIH}}^2 = \omega_{c1} \omega_{c2} \frac{\beta_1 \omega_{c2} + \beta_2 \omega_{c1}}{\beta_1 \omega_{c1} + \beta_2 \omega_{c2}} , \quad (\text{B.5})$$

where

$$\beta_j = \frac{n_j}{n_e} .$$

Under the conditions

$$\mathcal{D} \approx 0 \quad ; \quad |\mathcal{D}^2 (k_{\perp}^2 - \rho)| \ll |\rho k_{\perp}^4| , \quad (\text{B.6})$$

eq. (B.1) becomes, for the ion cyclotron wave,

$$k_{\parallel}^2 = \frac{\mathcal{D}^2}{k_{\perp}^2} \left( 1 - \frac{k_{\perp}^2}{\rho} \right) . \quad (\text{B.7})$$

Therefore at the ion-ion hybrid resonance the parallel wavenumber, while still being finite, has a value different from that given by eq. (B.4). However, if the difference in mass of the two ion species is small, i.e.,  $\omega_{c1} \approx \omega_{c2}$ , then

$$\mathcal{D} \approx 0 \quad \text{at} \quad \omega = \omega_{\text{IIH}} \quad (\text{B.8})$$

and the conditions (B.6) are only satisfied then in a very narrow frequency band around the ion-ion hybrid frequency. For this band,

eq. (B.4) gives the value  $k_{\parallel}^2 \approx 0$  and hence close to the more accurate value determined by eq. (B.7). Therefore (B.4) may be used to calculate the parallel wavenumber to a good approximation throughout the entire frequency regime of interest.

An approximate radial boundary condition at the plasma-vacuum interface can be obtained by examining the wavefields for the parameter range under consideration. From eq. (18) and (20), in the vacuum region

$$b_{\theta}^n = -\frac{i}{\omega} k_{\parallel} \left( 1 - \frac{k_0^2}{k_{\parallel}^2} \right) e_r^n . \quad (\text{B.9})$$

Now

$$\left( 1 - \frac{k_0^2}{k_{\parallel}^2} \right) = \frac{\omega^2}{k_{\parallel}^2 c^2} = \frac{1}{n_{\parallel}^2} \ll 1 \quad (\text{B.10})$$

since the free space wavelength is much greater than the wavelength in the plasma. (For the parameters listed in (31), the square of the parallel plasma refractive index is  $n_{\parallel}^2 = 2.6 \times 10^5$ .) Condition (B.10) is equivalent to assuming that the vacuum displacement current may be neglected in the vacuum region and yields, from eq. (B.9),

$$b_{\theta}^n (\text{vacuum}) \approx 0 . \quad (\text{B.11})$$

Now, in the plasma region,

$$b_{\theta}^n(r) = -\frac{i}{\omega} \left\{ (k_{\parallel} + k_{11} \epsilon_{31}) A_1^n J_1(k_{11} r) + (k_{\parallel} + k_{12} \epsilon_{32}) A_2^n J_1(k_{12} r) \right\} .$$

Substituting from eq. (15) and (B.3)

$$b_{\theta}^n(r) \approx -\frac{i}{\omega} k_{\parallel} \left\{ \frac{\mathcal{A}}{k_{\parallel}^2} A_1^n J_1(k_{11} r) + A_2^n J_1(k_{12} r) \right\} .$$

However, since  $\epsilon_{21}/\epsilon_{22} \approx 0$ , from eq. (12) and (16) the requirement that the fields in the plasma are finite implies that  $A_2^n/A_1^n \approx 0$ . Hence

$$b_{\theta}^n(r) \approx -\frac{i}{\omega} \frac{\mathcal{D}}{k_{\perp}} A_1^n J_1(k_{\perp} r). \quad (\text{B.12})$$

Continuity of the magnetic field component across the plasma-vacuum interface (since there exists no surface currents) then yields the approximate boundary condition

$$J_1(k_{\perp} \rho) = 0,$$

or

$$k_{\perp} \rho = \alpha_{\ell}, \quad (\text{B.13})$$

where  $\alpha_{\ell}$  is the  $\ell^{\text{th}}$  zero of the  $J_1$  Bessel function. The subscript  $\ell$  denotes here the radial mode number.

Now, from eq. (6),  $\mathcal{D}$  and  $\mathcal{P}$  may be approximated, for frequencies in the vicinity of the ion cyclotron frequency, by

$$\mathcal{D} \approx \frac{\omega^2}{c^2} \left( 1 + \frac{\omega_{pe}^2}{\Omega^2} \right) \quad (\text{B.14a})$$

$$\mathcal{P} \approx \frac{\omega^2}{c^2} \left( 1 - \frac{\omega_{pe}^2}{\omega^2} \right), \quad (\text{B.14b})$$

where, for a plasma containing two ion species,

$$\Omega^2 = \left[ \sum_{j=1}^2 \frac{m_e}{m_j} \beta_j (\omega_{cj}^2 - \omega^2)^{-1} \right]^{-1}. \quad (\text{B.15})$$

We shall assume that the ions of the minority species have the heaviest mass (as in the case of naturally occurring  $\text{Ne}^{20}$  and  $\text{Ne}^{22}$ ), so that  $\Omega^2$  is positive, and also that the inequality

$$\frac{c^2}{\Omega^2} \frac{\alpha_e^2}{p^2} \gg 1$$

is well satisfied (as is the case for the parameters listed in (31)).

The relationship between the parallel wavenumber and the electron density, given by eq. (B.4), can be considered in four different density regimes.

I) very low density:  $\omega^2 \lesssim \omega_{pe}^2$

Since  $\rho \approx 0$  for this region,  $k_{\parallel}^2$  is very large. This is a manifestation of the plasma cutoff<sup>8</sup>.

II) Low density :  $\omega^2 \ll \omega_{pe}^2 \ll \Omega^2$

For this region

$$\delta \approx \frac{\omega^2}{c^2}$$

$$\rho \approx - \frac{\omega_{pe}^2}{c^2} ,$$

$$\text{and } k_{\parallel}^2 \approx - \frac{\delta}{\rho} k_{\perp}^2 = \frac{\omega^2}{\omega_{pe}^2} \frac{\alpha_e^2}{p^2} . \quad (\text{B.16})$$

Therefore,  $k_{\parallel}^2 \propto n_e^{-1}$ .



III) moderate density :  $\Omega^2 \ll \omega_{pe}^2 \ll k_{\perp 1}^2 c^2$

For this region

$$\delta \approx \frac{\Omega^2}{c^2} \frac{\omega_{pe}^2}{k_{\perp 1}^2}$$

$$\rho \approx - \frac{\omega_{pe}^2}{c^2} ,$$

$$\text{and } k_{\parallel}^2 \approx - \frac{\delta}{\rho} k_{\perp 1}^2 = \frac{\Omega^2}{k_{\perp 1}^2} \frac{k_{\perp 1}^2}{\omega_{pe}^2} . \quad (\text{B.17})$$

Therefore,  $k_{\parallel}^2$  is independent of  $n_e$ .

IV) high density :  $\omega_{pe}^2 \gg k_{\perp 1}^2 c^2$

$$\text{Here, } k_{\parallel}^2 \approx \delta = \frac{\Omega^2}{c^2} \frac{\omega_{pe}^2}{k_{\perp 1}^2} . \quad (\text{B.18})$$

Therefore,  $k_{\parallel}^2$  is proportional to  $n_e$ .

It can be noted that the last inequality may be written as  $\lambda_{\perp} \gg \delta$ , where  $\delta = c/\omega_{pe}$  is the collisionless skin depth. Thus finite electron inertia effects do not play a significant role in the wave behaviour (and therefore,  $E_z = 0$ ) if the wave scale length in the radial direction is much greater than the collisionless skin depth.

Each of the regions I to IV can be identified in Fig. 5. In particular, for the parameters listed in (31), we have

$$\Omega^2 \ll \omega_{pe}^2 \ll k_{\perp 1}^2 c^2 ,$$

and therefore  $k_{\parallel}$  is independent of  $n_e$ . In addition, eq. (B.17) shows that  $k_{\parallel}$  is inversely proportional to  $p$ , as is verified by Fig. 4.

REFERENCES

1. Hooke, W.M., Tenney, F.H., Brennan, M.H., Hill, H.M. and Stix, T.H. (1961) Phys. Fluids, 4, 1131.
2. Yoshikawa, S., Rothman, M.A. and Sinclair, R.M. (1965) Phys. Rev. Lett. 14, 214.
3. Rothman, M.A., Sinclair, R.M. and Yoshikawa, S. (1966) Plasma Phys. 8, 241.
4. Yoshikawa, S., Sinclair, R.M. and Rothman, M.A. (1966) Plasma Phys. and Contr. Nucl. Fusion Research, II, 925.
5. Hosea, J.C. and Sinclair, R.M. (1969) Phys. Rev. Lett. 23, 3.
6. Rothman, M.A., Sinclair, R.M., Brown, I.G. and Hosea, J.C. (1969) Phys. Fluids, 12, 2211.
7. Hosea, J.C. and Sinclair, R.M. (1970) Phys. Fluids, 13, 701.
8. Stix, T.H. (1962) Theory of Plasma Waves (McGraw-Hill, New York).
9. Tran, M.Q., Kohler, P., Paris, P.J., and Sawley, M.L. (1982) Lausanne Report LRP 205/82.
10. Weibel, E.S. (1980) Phys. Rev. Lett. 44, 377.
11. Festeau-Barrioz, M.C. and Weibel, E.S. (1980) Phys. Fluids, 23, 2045.
12. Weibel, E.S. and Festeau-Barrioz, M.C. (1982) Plasma Phys. 24, 243.
13. Skipping, C.R., Oakes, M.E. and Schlüter, H. (1969) Phys. Fluids, 12, 1886.

References (cont'd)

14. Schlüter, H. and Schürger, G. (1975) Z. Naturforsch. 30a, 1600.
15. Jackson, J.D. (1975) Classical Electrodynamics (Wiley, New York) p. 241.
16. Toyama, H. and Matsuura, K. (1973) Nucl. Fusion, 13, 363.
17. Braginskii, S.I. (1965) Reviews of Plasma Physics (ed. M.A. Leontovich) 1, 205.
18. Spitzer, L. (1962) Physics of Fully Ionized Gases (Interscience, New York).
19. Brennan, M.H. and Morrow, R. (1971) J. Phys. B., 4, L53.
20. Tanenbaum, B.S. (1967) Plasma Physics (McGraw-Hill, New York).
21. Rapp, D. and Francis, W.E. (1962) J. Chem. Phys. 37, 2631.
22. Buchsbaum, S.J. (1960) Phys. Fluids, 3, 418.

FIGURE CAPTIONS

- Fig. 1. Schematic diagram of the partially plasma-filled cavity.
- Fig. 2. Relationship between the parallel and perpendicular wavenumbers for a plasma with parameters given in (31) and a frequency of  $\omega = 1.372 \times 10^6$  rad s<sup>-1</sup>. The dashed curves give the asymptotic limits for the slow wave branch.
- Fig. 3. Parallel wavenumber,  $k_{\parallel}$ , as a function of the wave frequency,  $\omega$ , for the ion cyclotron wave in the vicinity of the ion cyclotron frequencies of the two ion species plasma. Curves are shown for the lowest four radial modes.
- Fig. 4. Parallel wavenumber,  $k_{\parallel}$ , as a function of the plasma radius,  $\rho$ , for the lowest four radial modes.
- Fig. 5. Parallel wavenumber,  $k_{\parallel}$ , as a function of the electron density,  $n_e$ , for the lowest four radial modes.
- Fig. 6. Enlargement of a section of Fig. 3 illustrating graphical determination of the oscillation frequencies for the lowest order eigenmodes.
- Fig. 7. Radial and axial profiles of the amplitude of (a) the electric field, and (b) the magnetic field components for the ( $n = 4$ ,  $\ell = 1$ ) eigenmode. The radial plots are shown at the respective axial antinodes of the fields, while the axial plots are shown at the radial position of maximum field amplitude. The amplitude of the fields are normalized to provide an axial electric field of  $10 \text{ Vm}^{-1}$  on the plasma axis at the axial antinodes.
- Fig. 8. Eigenfrequency for the ( $n = 4$ ,  $\ell = 1$ ) mode as a function of the percentage concentration of the  $\text{Ne}^{20}$  species. The value calculated for the natural concentration is marked by a dot on the curve.

Figure captions (cont'd)

- Fig. 9. Schematic diagram of the antenna structure assumed for the forced oscillation calculations.
- Fig. 10. Fourier spectrum of (a) the antenna current and (b) the resistive power input to the plasma at a driving frequency of  $\omega = 1.381 \times 10^6 \text{ rad s}^{-1}$ .
- Fig. 11. Frequency dependence of the resistive and reactive power input to the plasma for the  $n = 4$  mode.
- Fig. 12. Radial and axial profiles of the amplitude of (a) the electric field, and (b) the magnetic field components for forced oscillation at a driving frequency of  $\omega = 1.381 \times 10^6 \text{ rad s}^{-1}$ . The fields are shown at the positions of maximum field amplitude.
- Fig. 13. Radial profiles of the amplitude of the electric and magnetic field components for forced oscillation at a driving frequency of  $\omega = 1.381 \times 10^6 \text{ rad s}^{-1}$  with the inclusion of a Faraday shield.
- Fig. 14. Resistive power input to the plasma at a driving frequency of  $\omega = 1.381 \times 10^6 \text{ rad s}^{-1}$  as a function of the radial position of the antenna. The value obtained for the antenna radius used in the previous calculations is indicated by a dot.
- Fig. 15. Fourier spectrum of (a) the antenna current, and (b) the resistive power input to the plasma at a driving frequency of  $\omega = 1.393 \times 10^6 \text{ rad s}^{-1}$  for a reduced cavity length of  $L = 4.75 \text{ m}$ .
- Fig. 16. Radial and axial profiles of the amplitude of the electric field components for forced oscillation at a driving frequency of  $\omega = 1.393 \times 10^6 \text{ rad s}^{-1}$  for a reduced cavity length of  $L = 4.75 \text{ m}$ .

$\omega$  ( $\times 10^6$  rad s $^{-1}$ )

n ↓	$\ell$ →			
	1	2	3	4
1	1.3288	1.3279	1.3277	1.3277
2	1.3344	1.3291	1.3283	1.3280
3	1.3524	1.3316	1.3293	1.3285
4	1.3809	1.3365	1.3309	1.3293
5	1.4016	1.3461	1.3334	1.3305
6	1.4145	1.3609	1.3375	1.3322

Table 1: Eigenfrequencies for the lowest order modes calculated for the parameters given in (31).

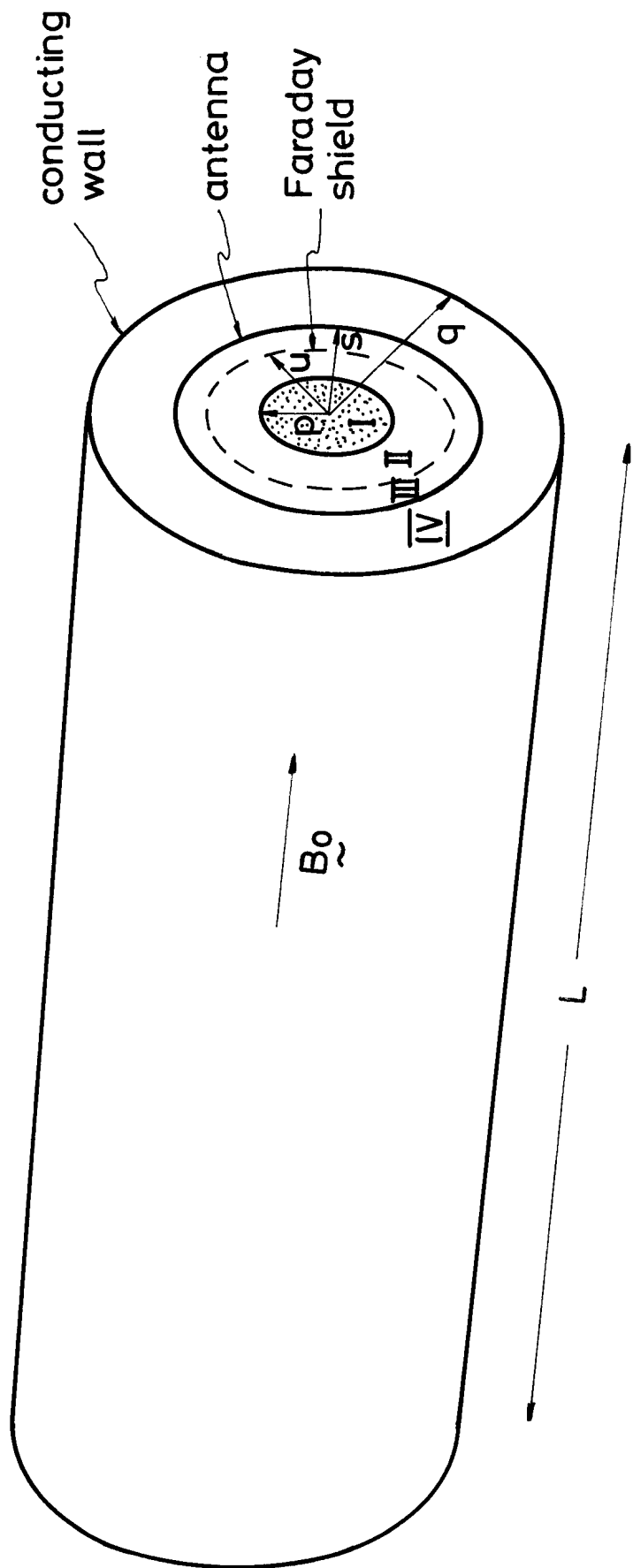


FIG. 1

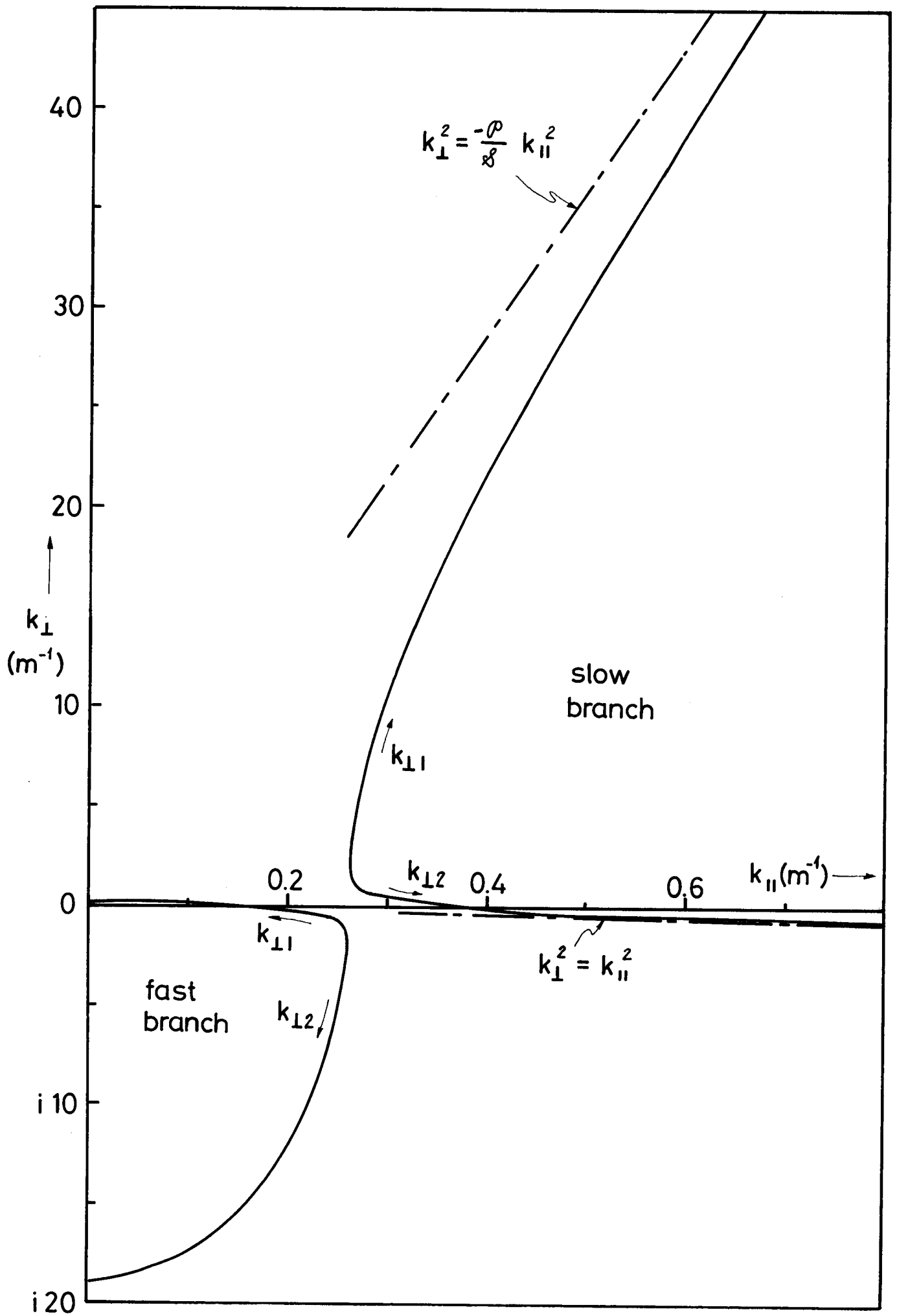


FIG. 2



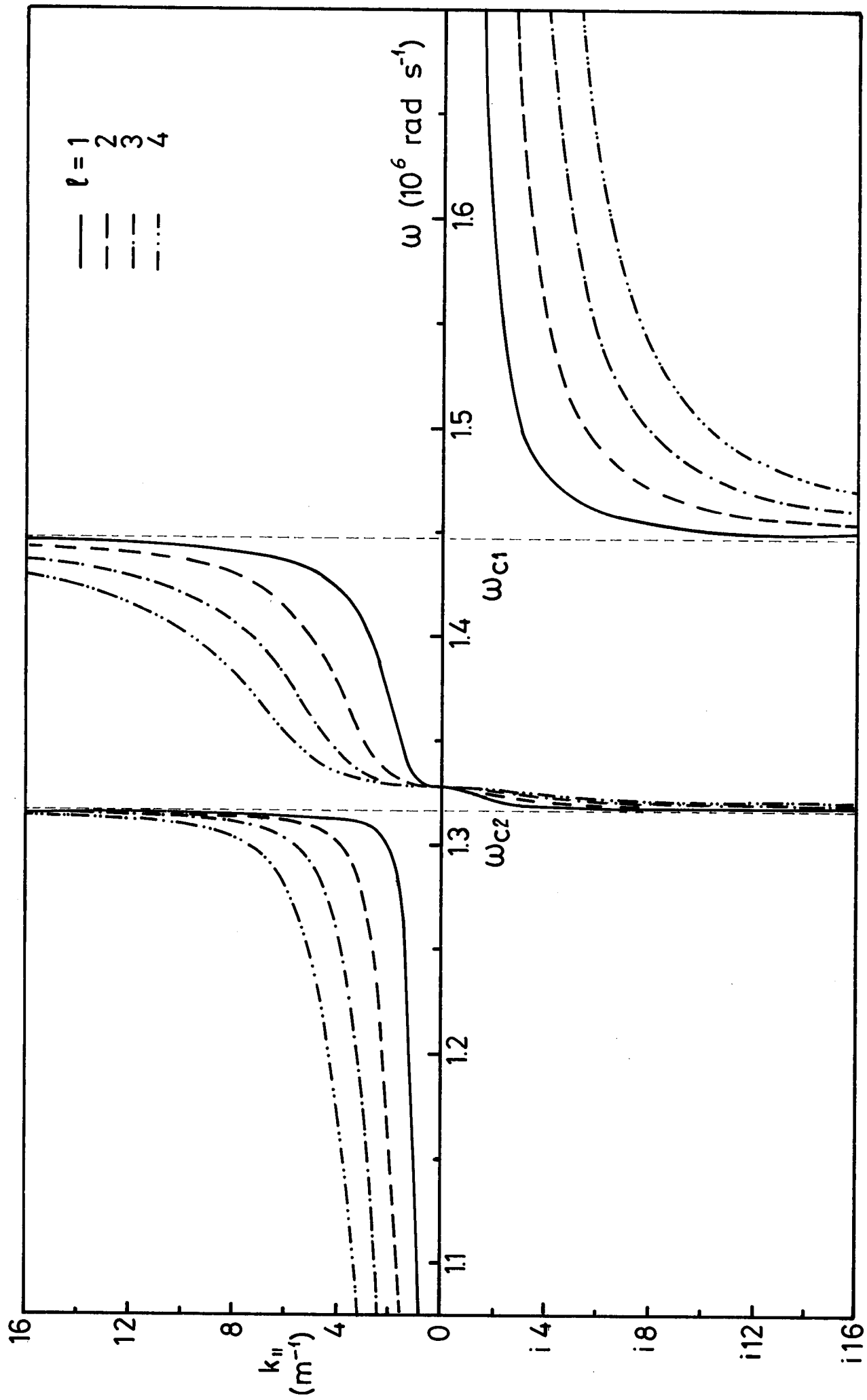


FIG. 3

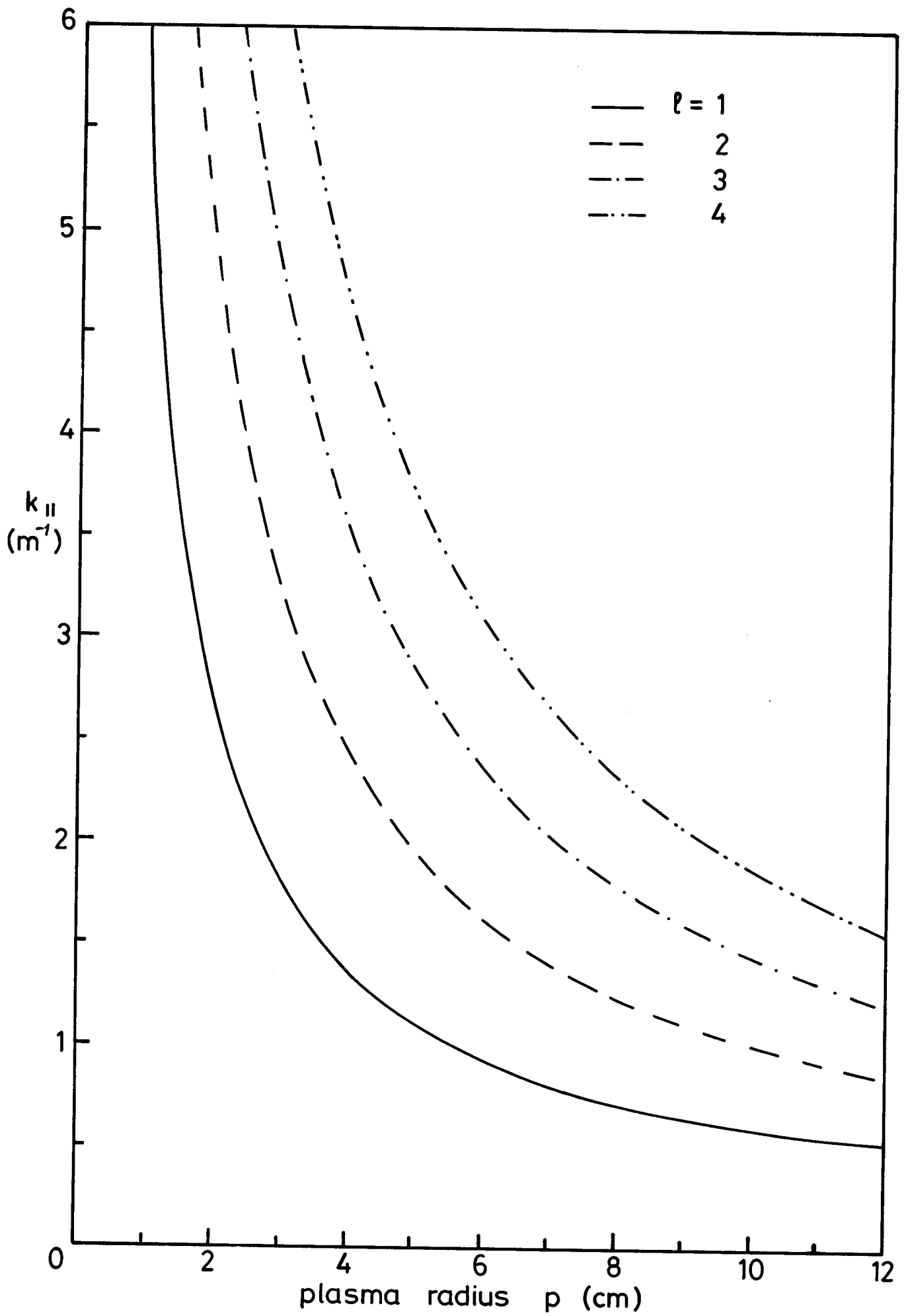


FIG. 4

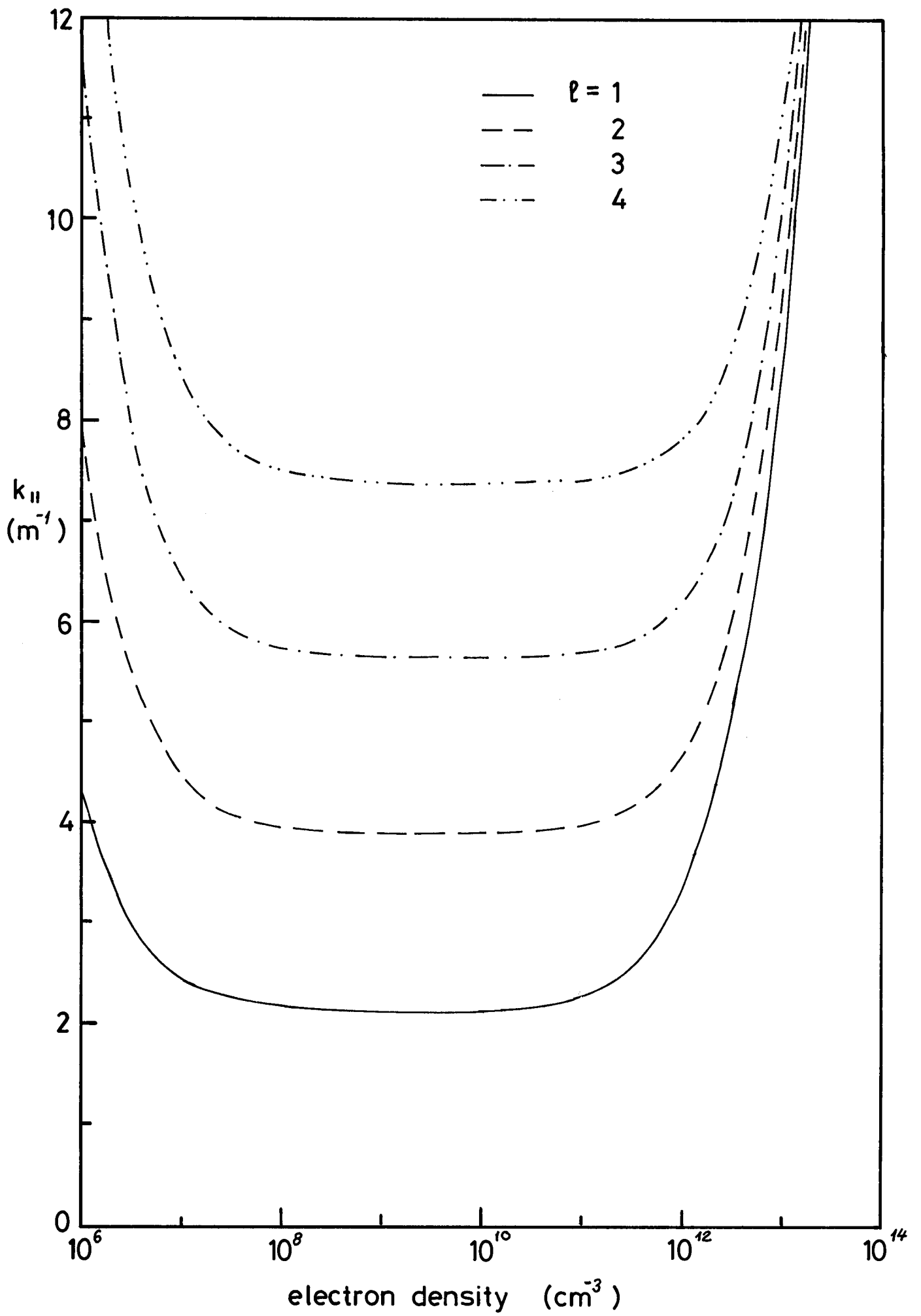


FIG. 5

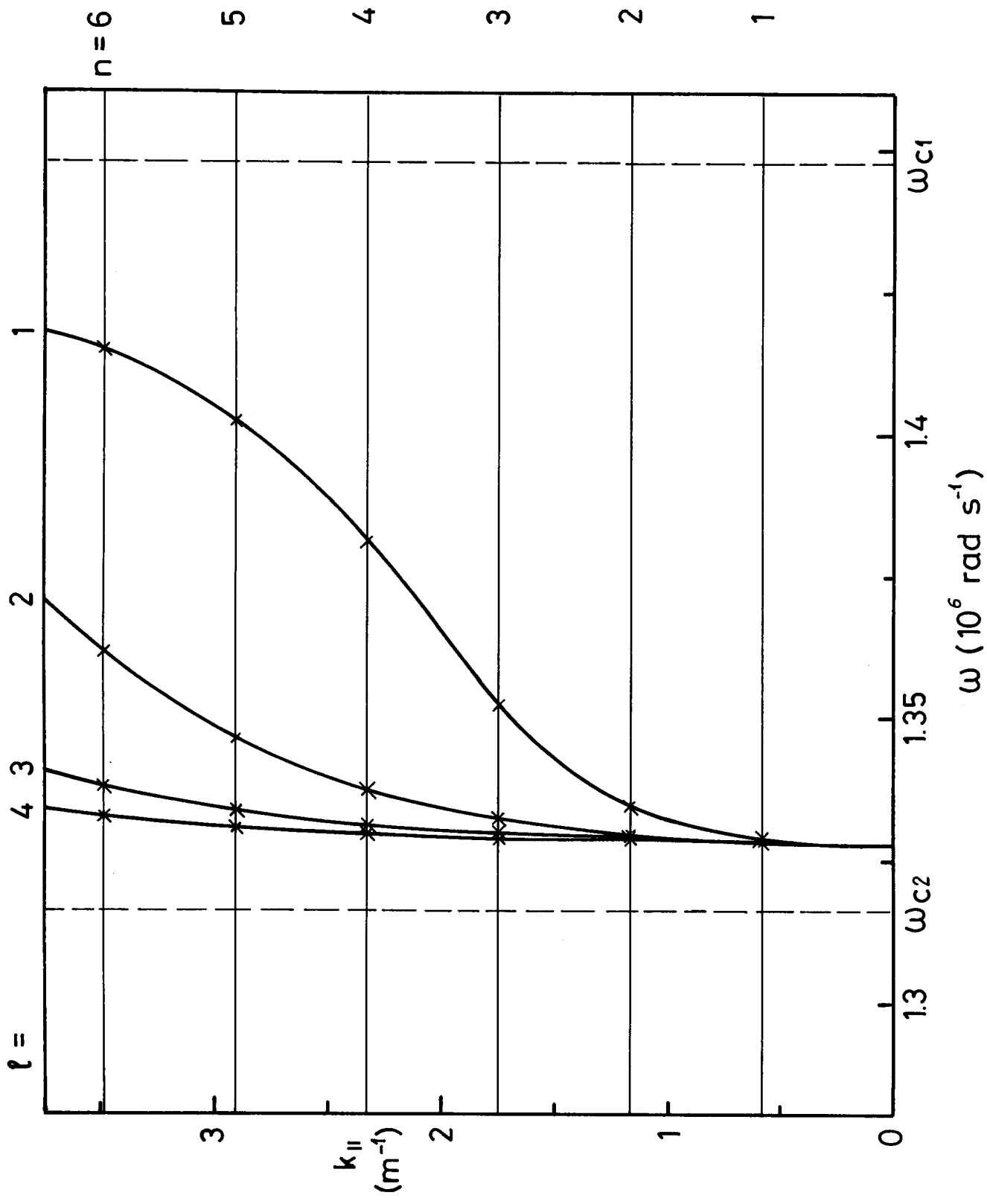


FIG. 6

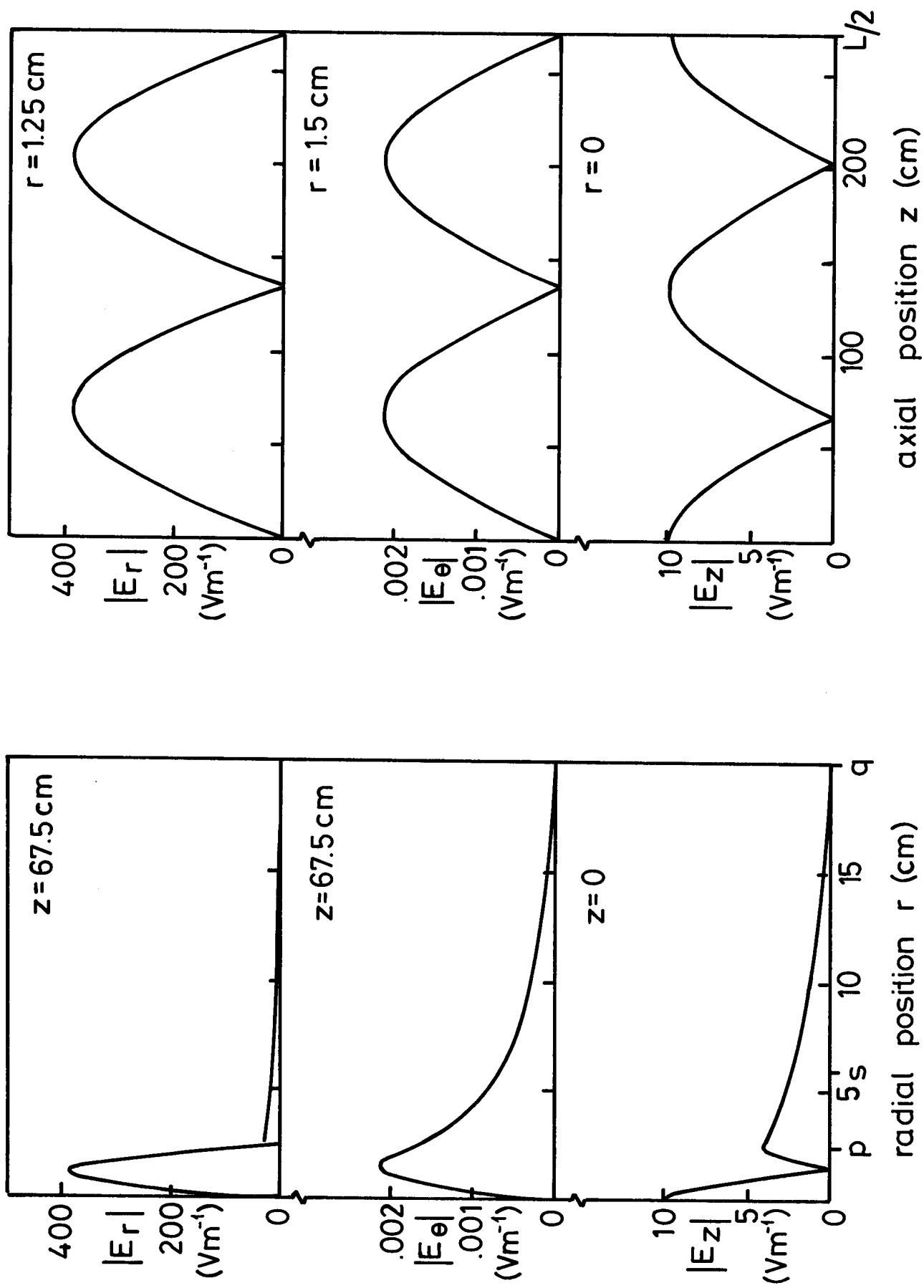


FIG. 7(a)

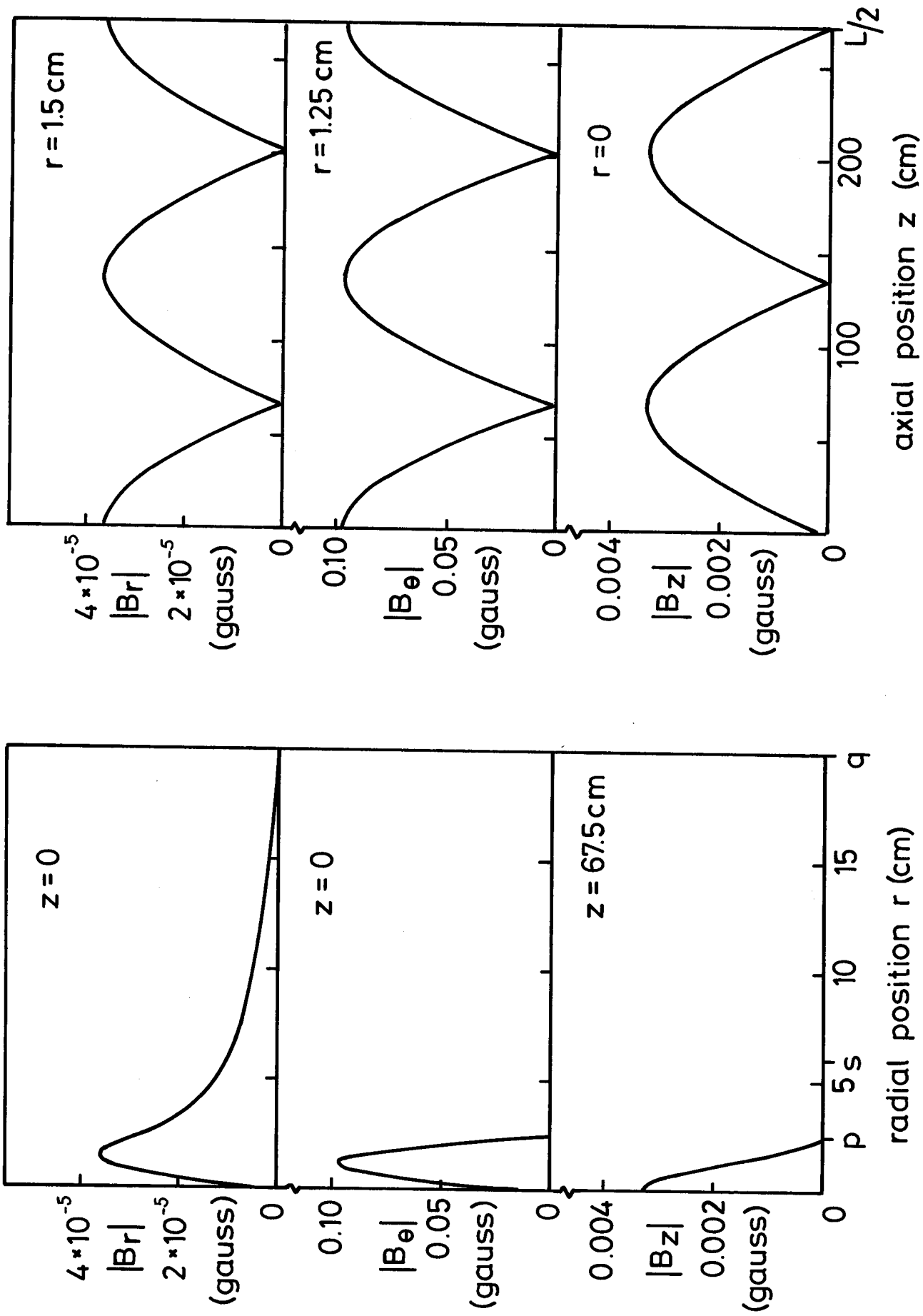


FIG. 7(b)

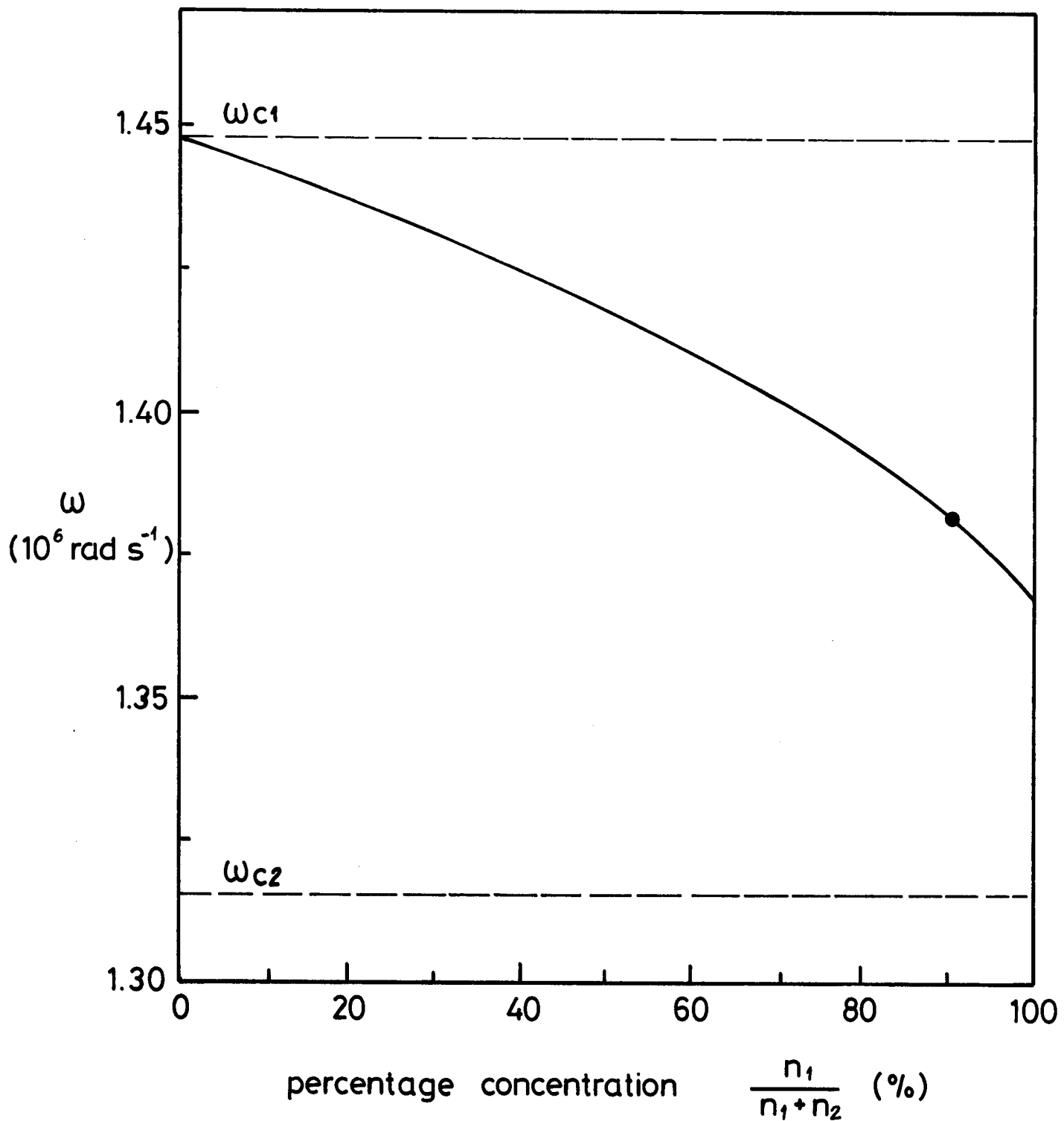


FIG. 8

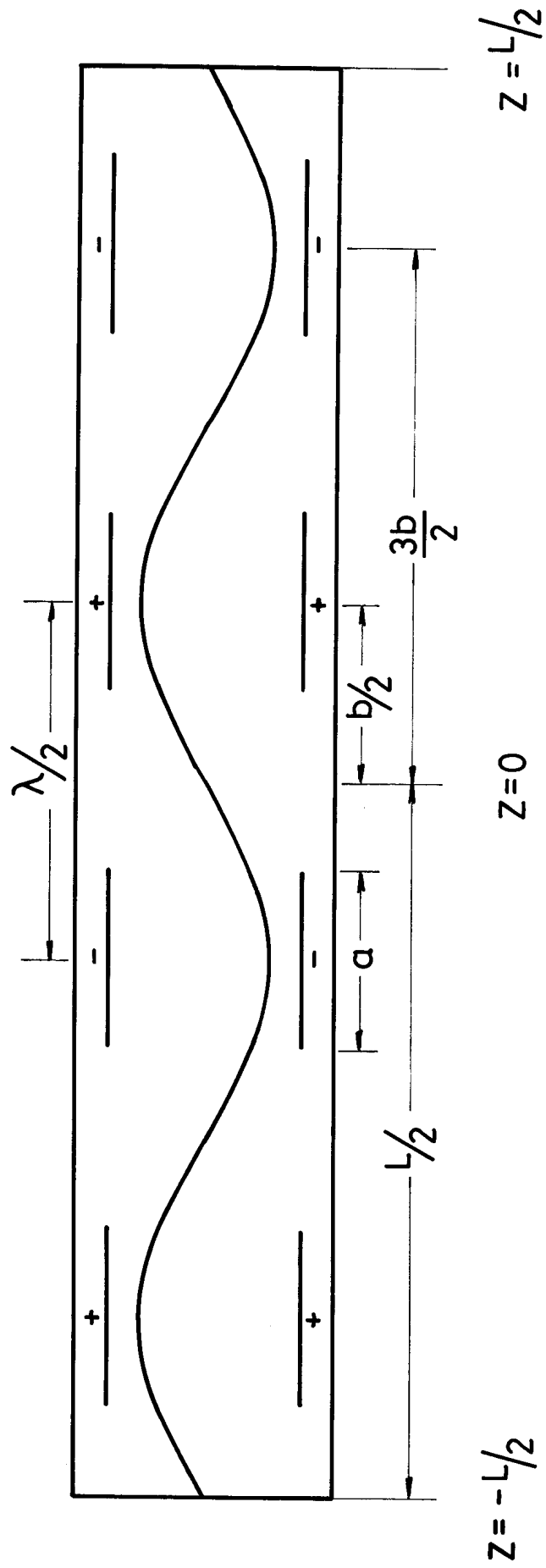


FIG. 9



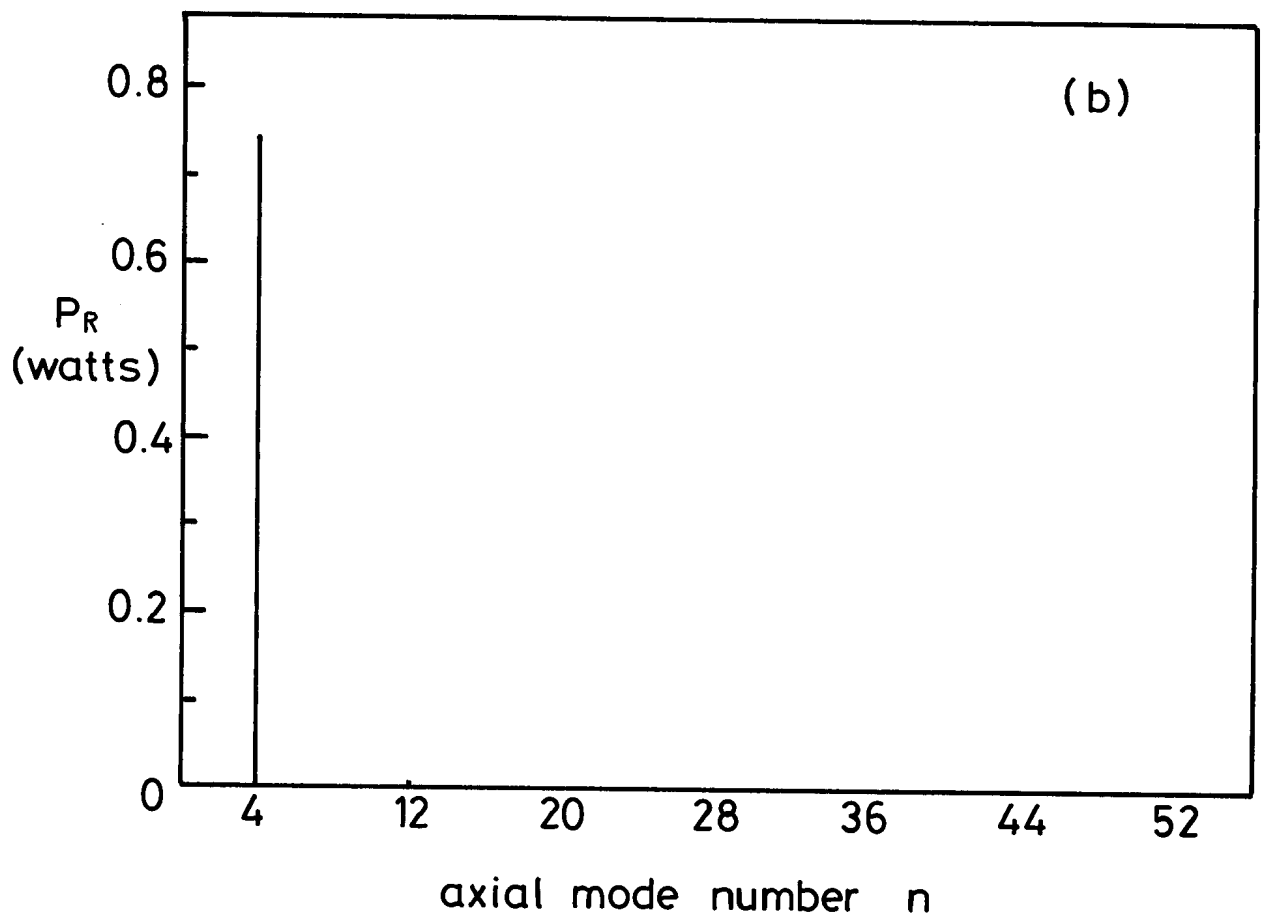
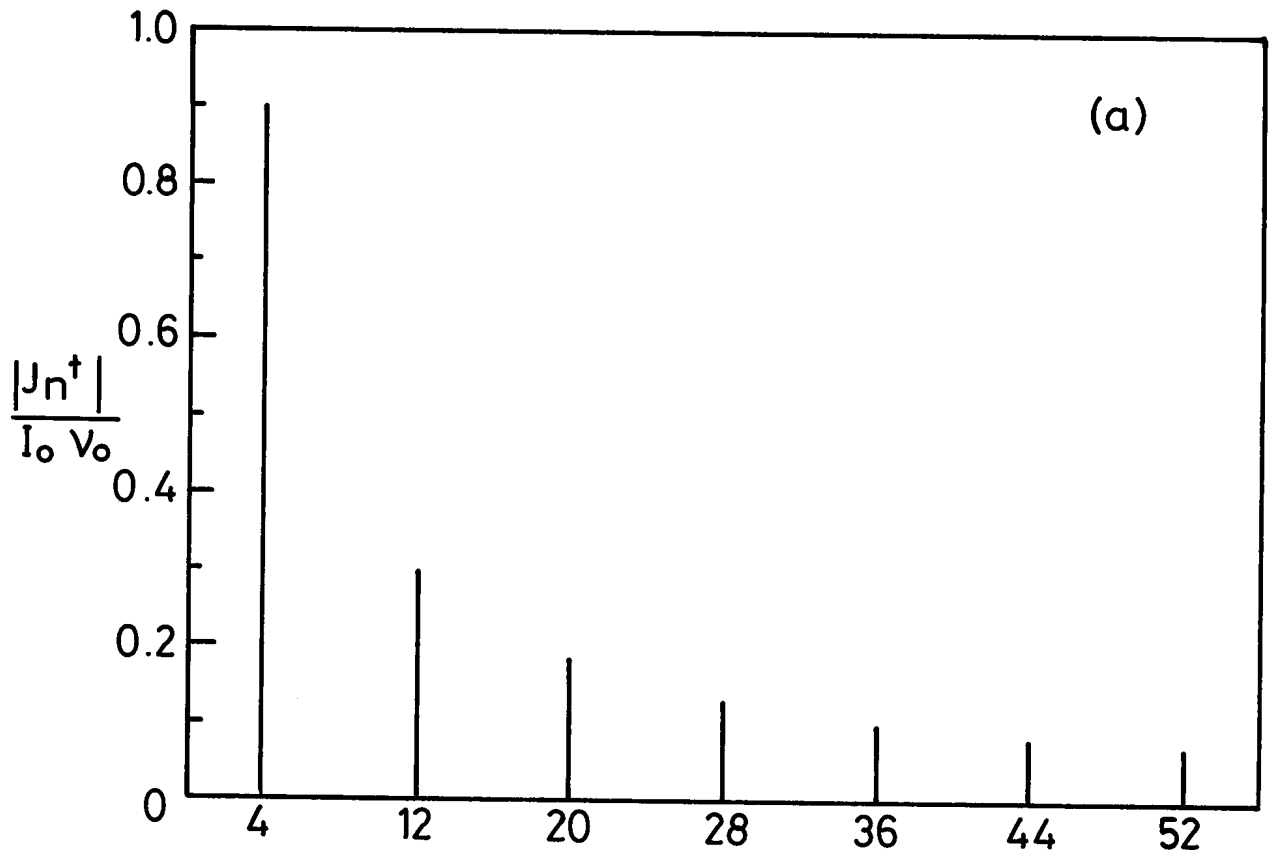


FIG. 10

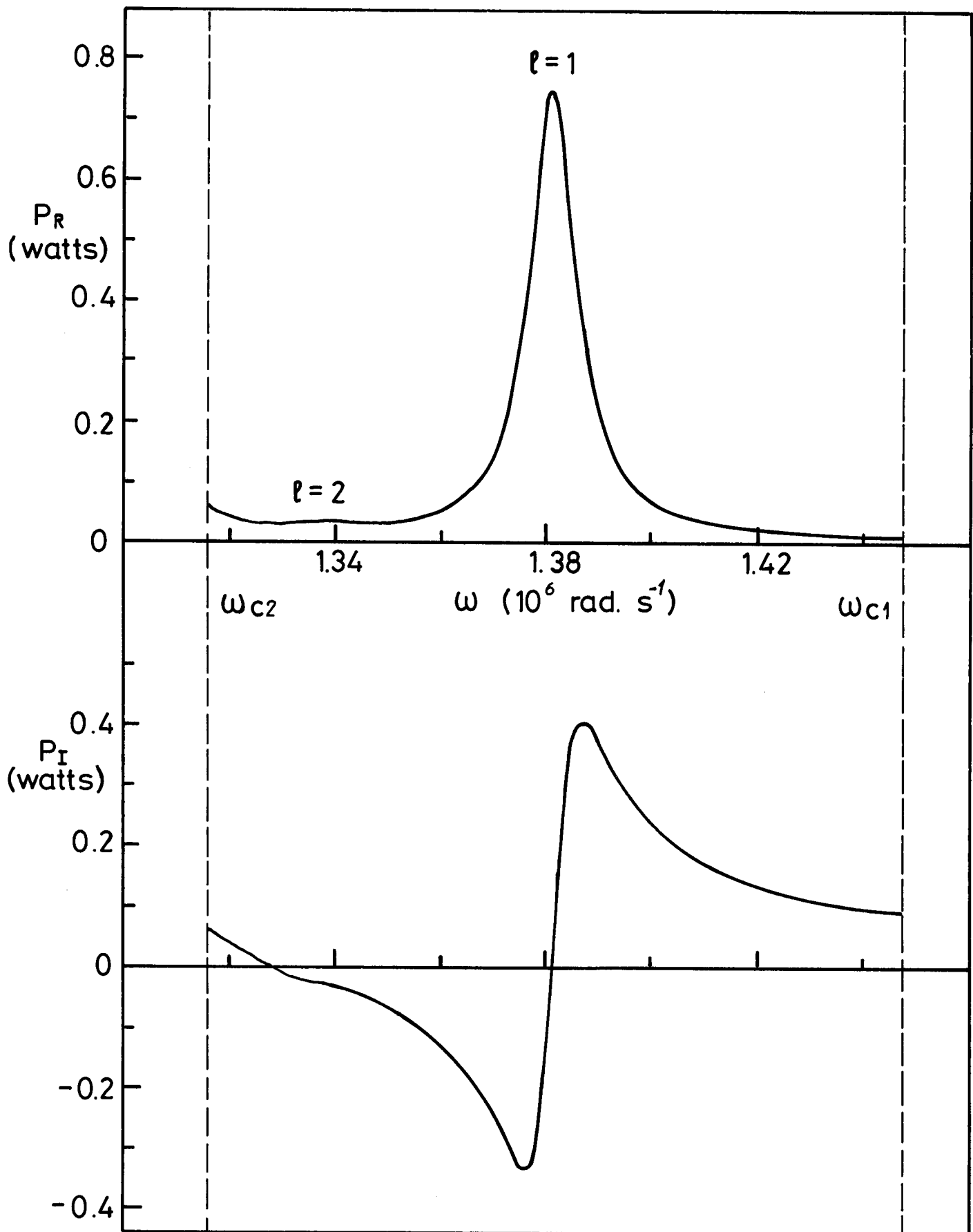


FIG. 11

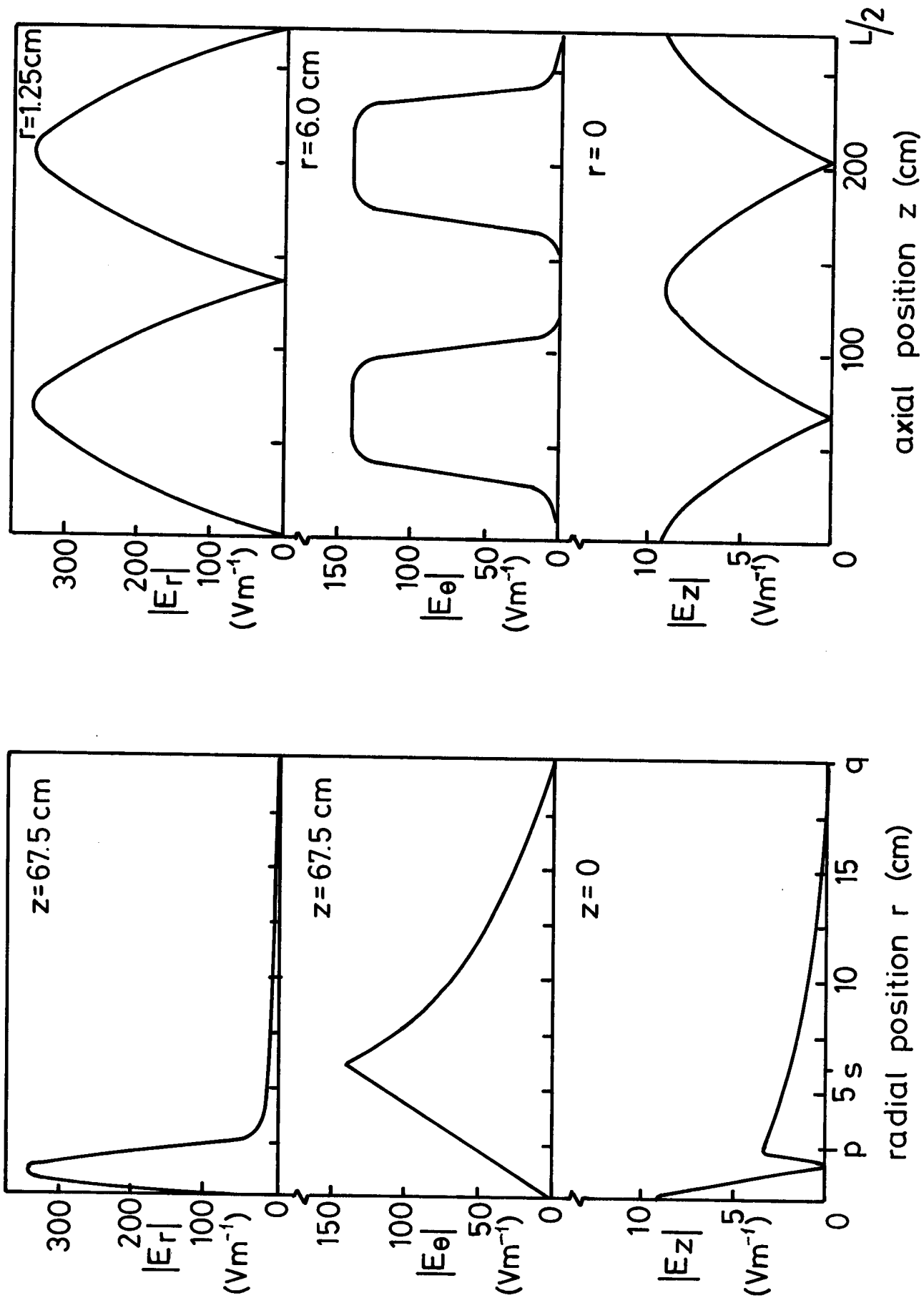


FIG. 12(a)

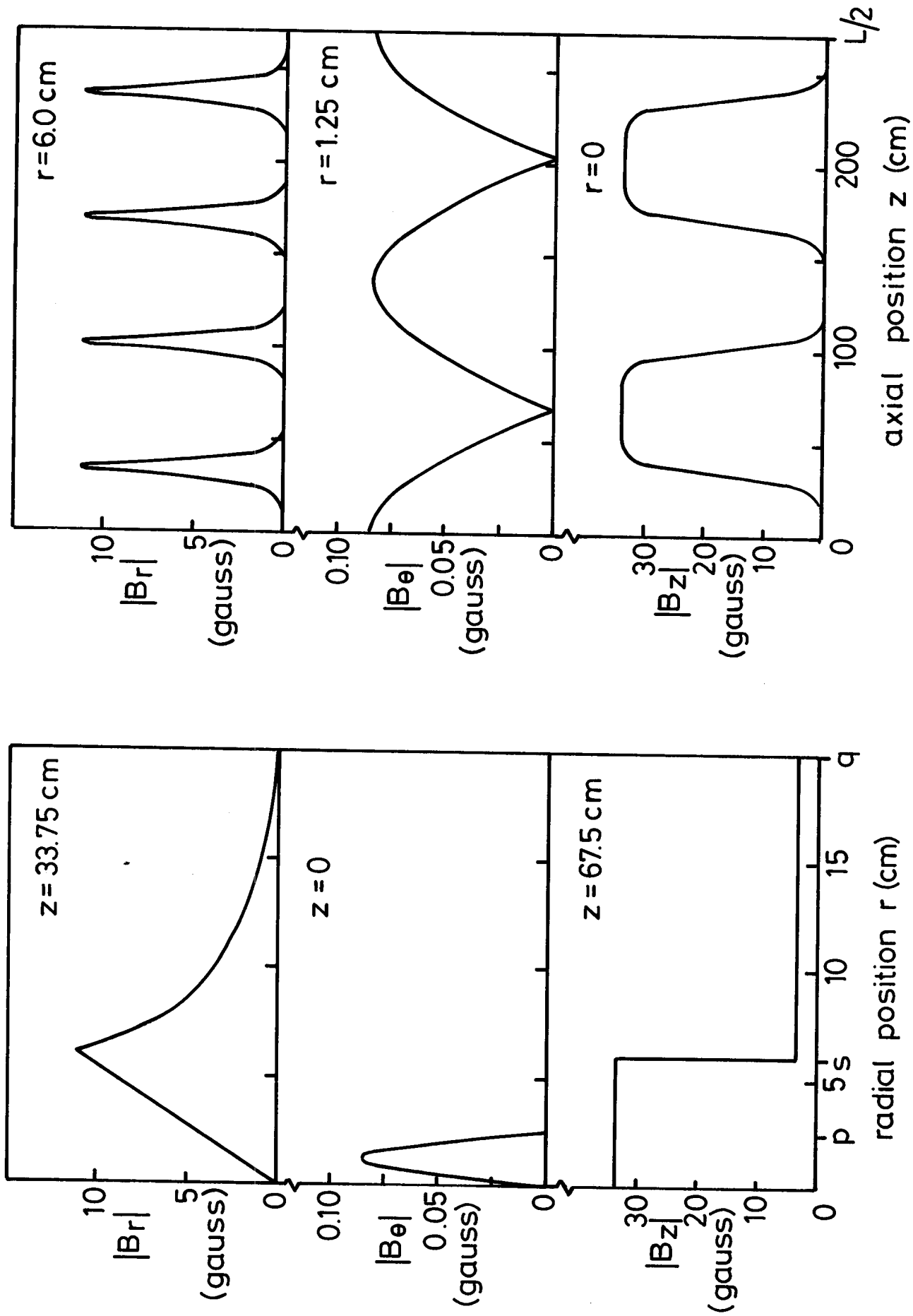


FIG. 12 (b)

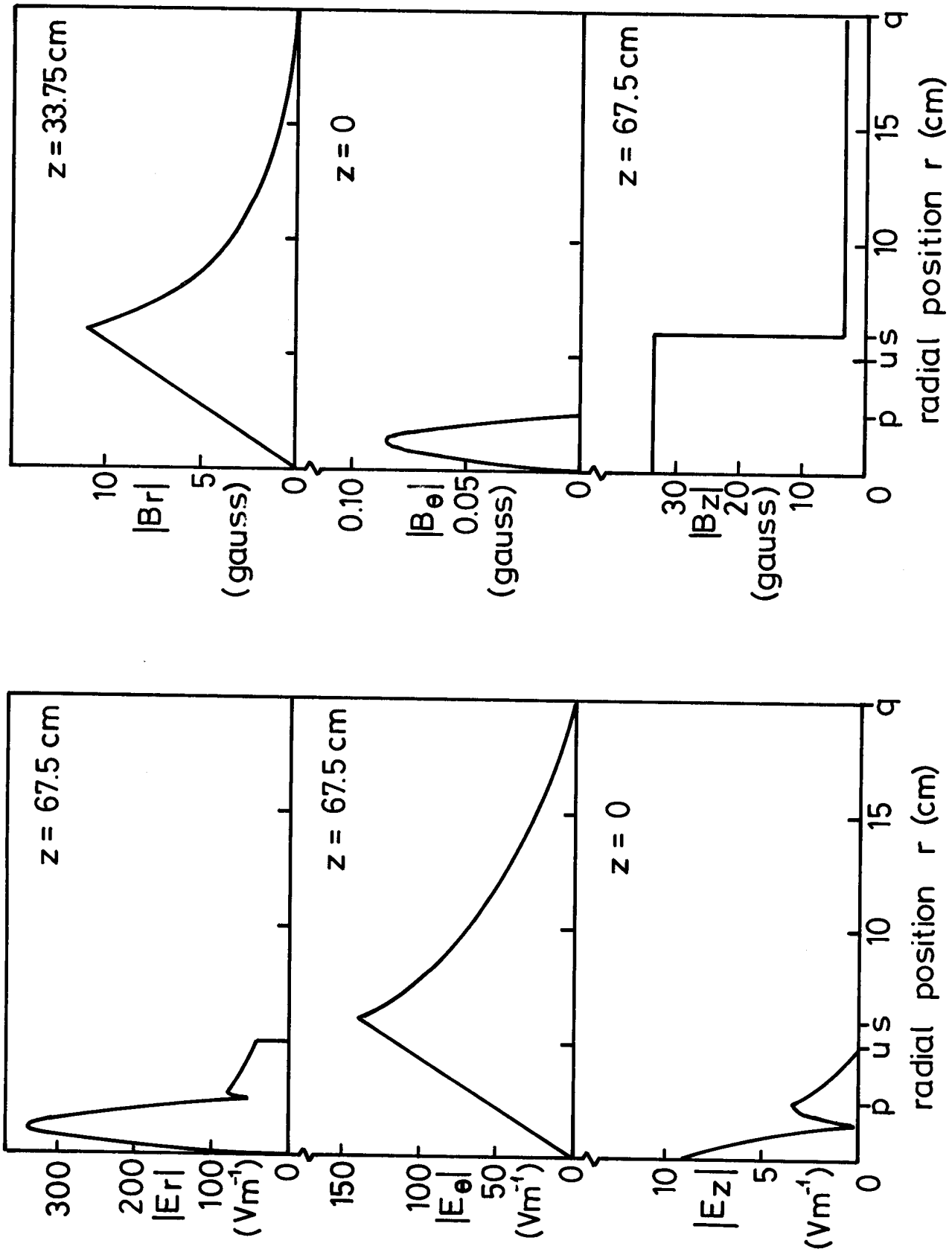


FIG. 13

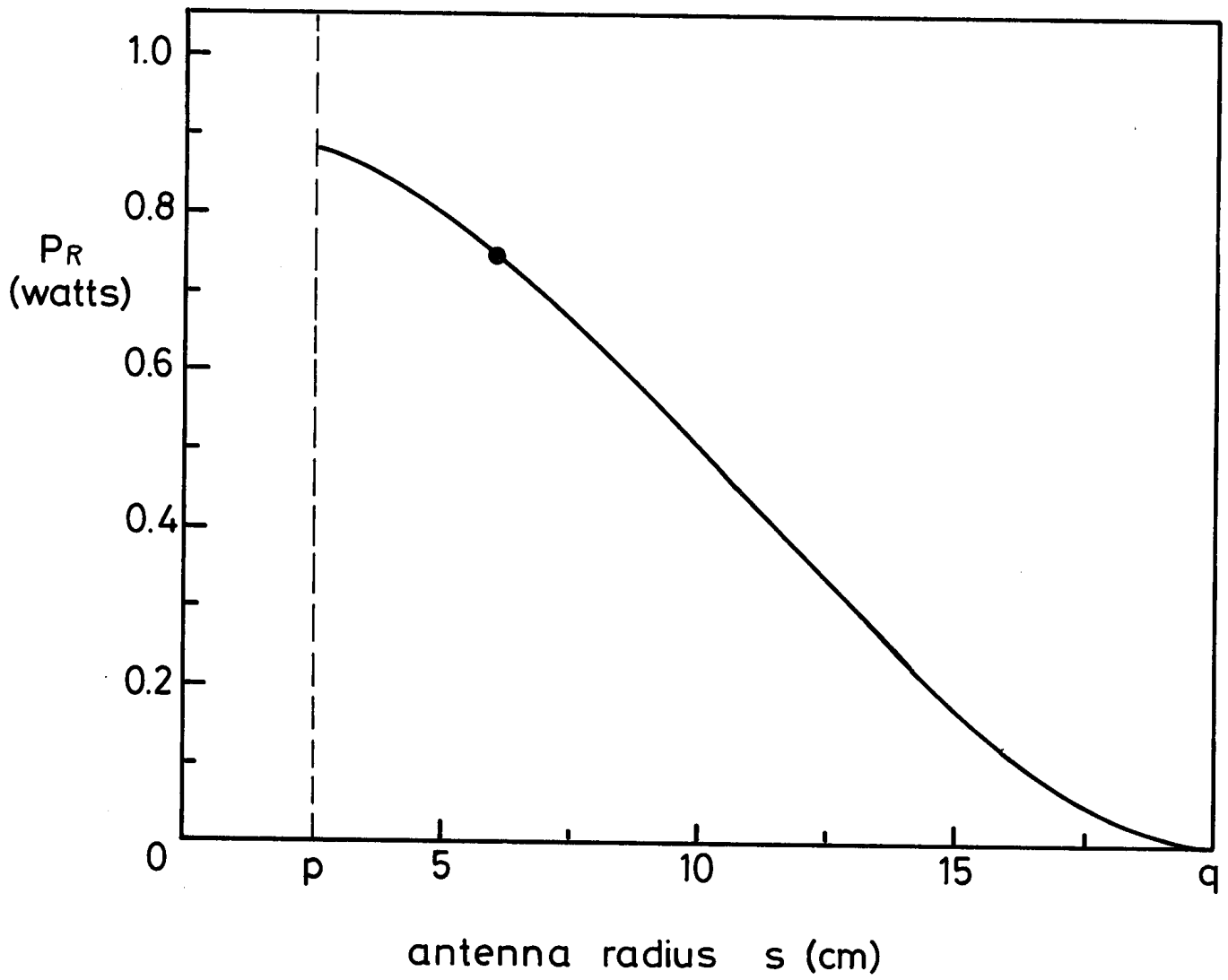


FIG.14

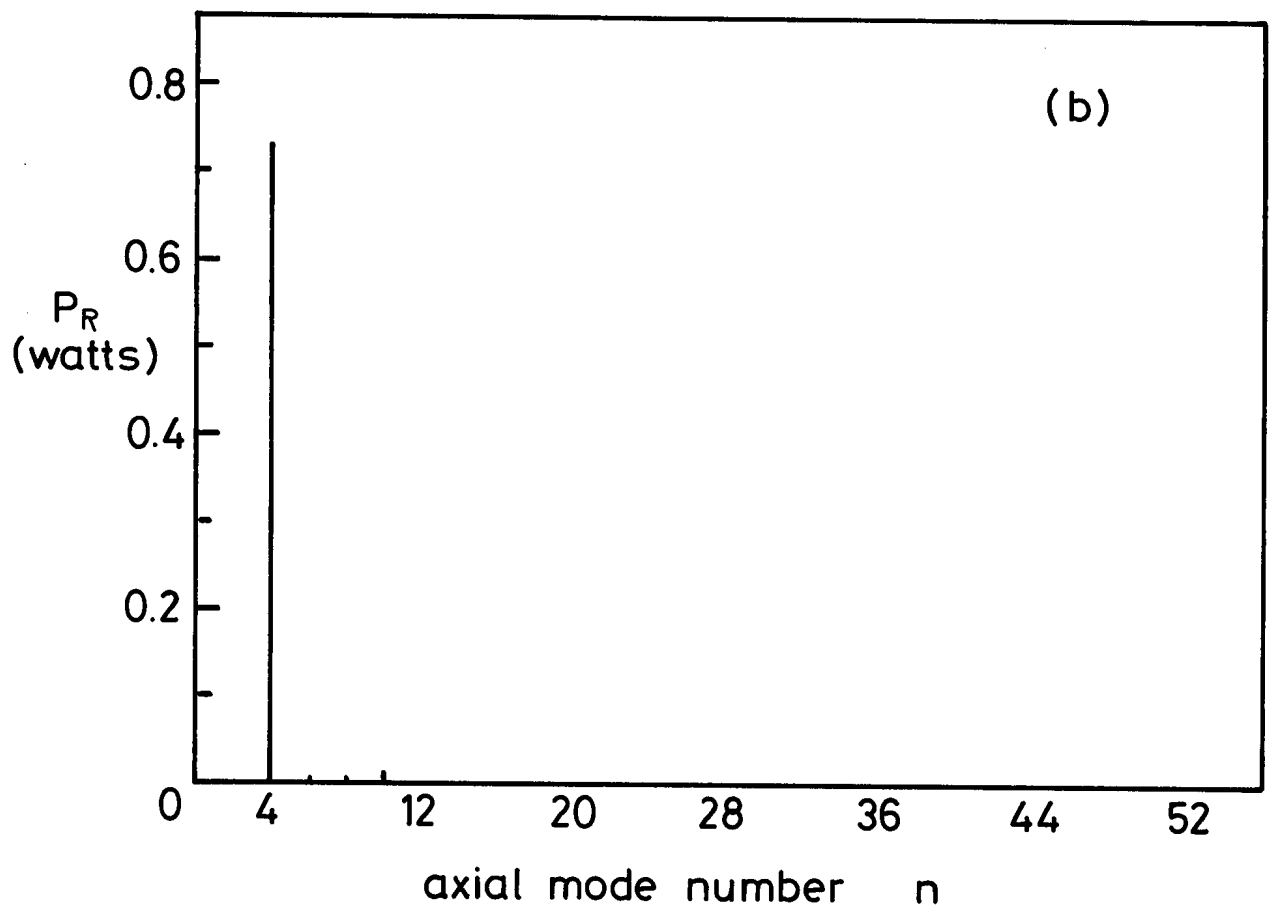
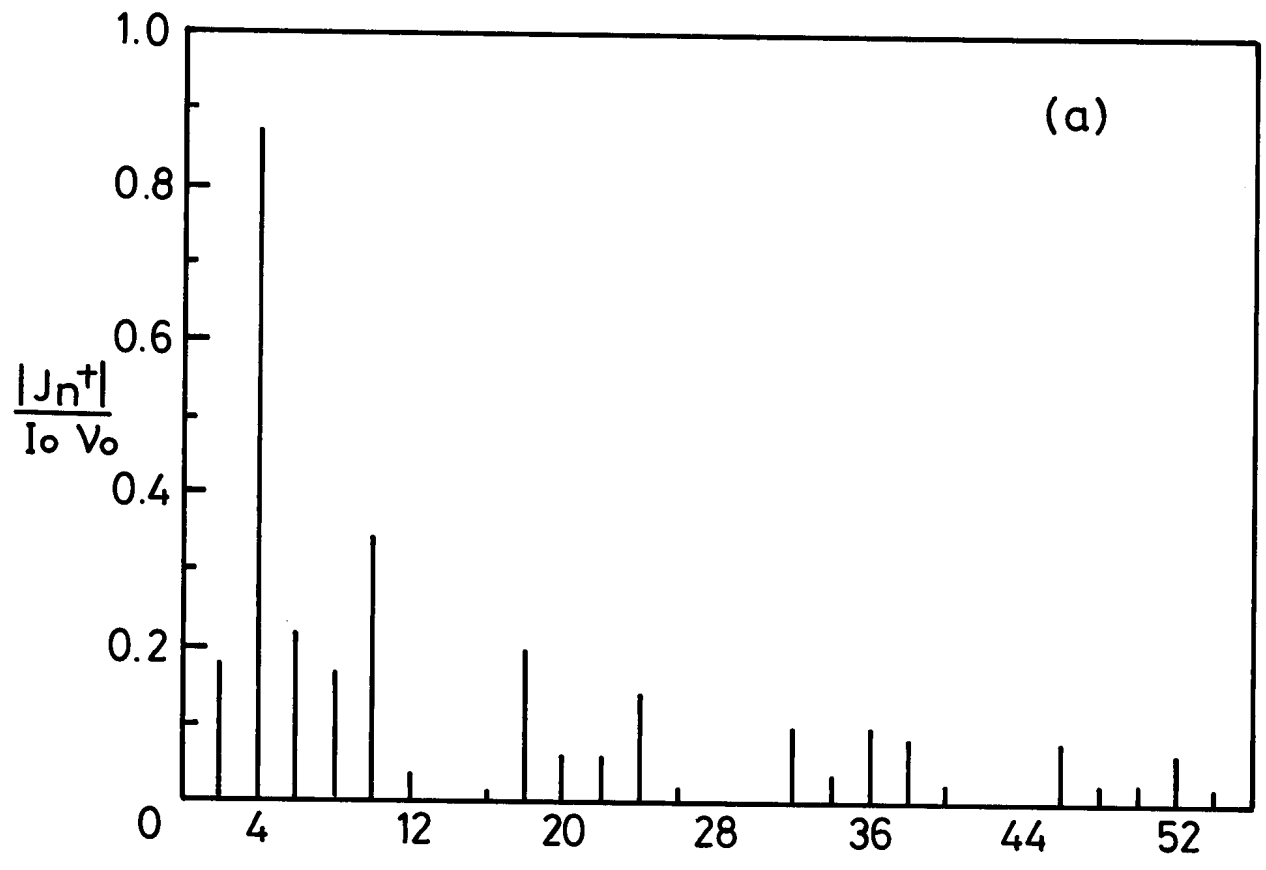


FIG. 15

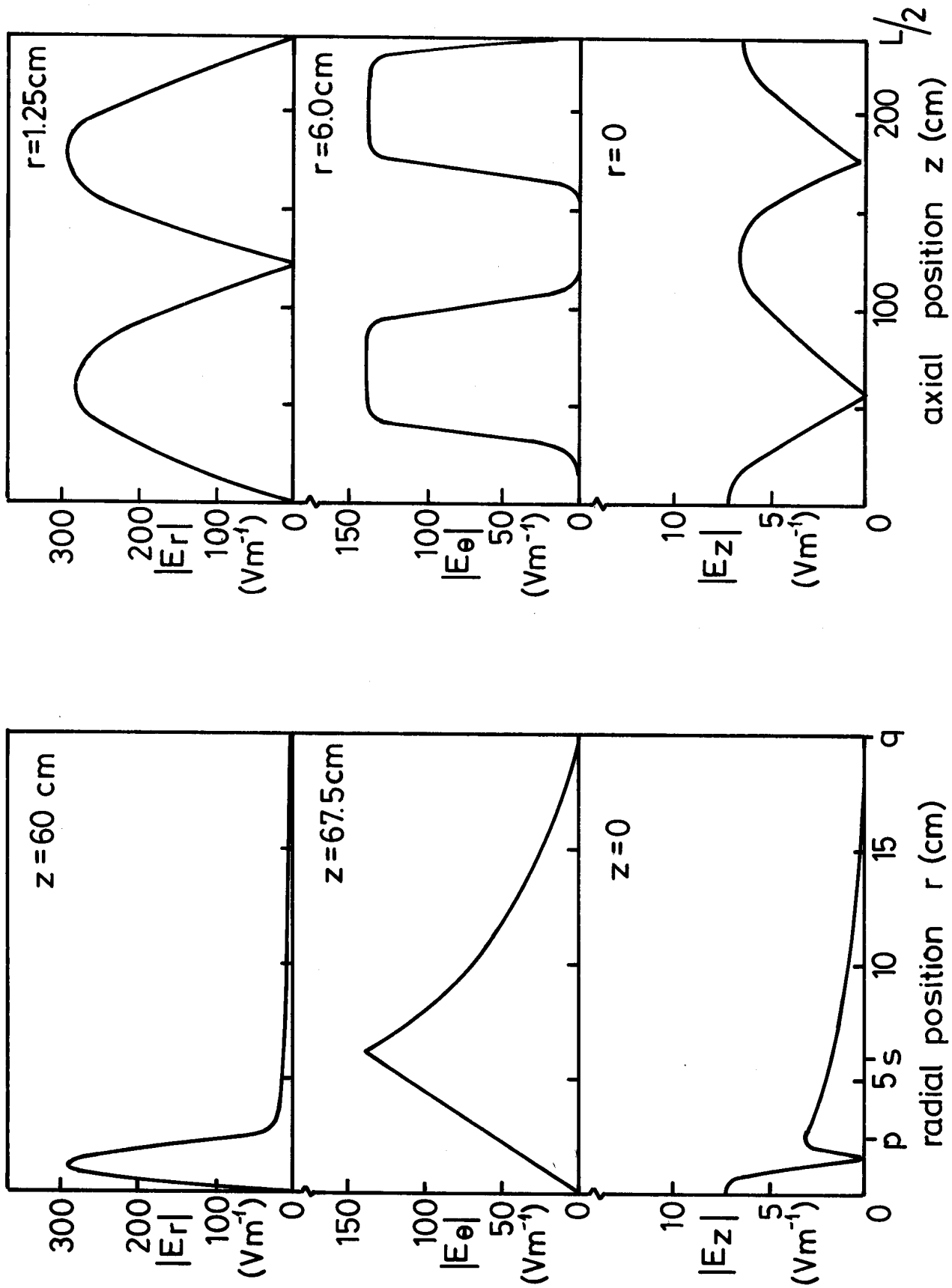


FIG. 16